



저작자표시-비영리-변경금지 2.0 대한민국

이용자는 아래의 조건을 따르는 경우에 한하여 자유롭게

- 이 저작물을 복제, 배포, 전송, 전시, 공연 및 방송할 수 있습니다.

다음과 같은 조건을 따라야 합니다:



저작자표시. 귀하는 원저작자를 표시하여야 합니다.



비영리. 귀하는 이 저작물을 영리 목적으로 이용할 수 없습니다.



변경금지. 귀하는 이 저작물을 개작, 변형 또는 가공할 수 없습니다.

- 귀하는, 이 저작물의 재이용이나 배포의 경우, 이 저작물에 적용된 이용허락조건을 명확하게 나타내어야 합니다.
- 저작권자로부터 별도의 허가를 받으면 이러한 조건들은 적용되지 않습니다.

저작권법에 따른 이용자의 권리는 위의 내용에 의하여 영향을 받지 않습니다.

이것은 [이용허락규약\(Legal Code\)](#)을 이해하기 쉽게 요약한 것입니다.

[Disclaimer](#)

Master Thesis

**Fabrication of Photocatalytic Thin Film by
Vacuum Kinetic Spray Method**

University of Ulsan

School of Mechanical engineering

SADDAM HOSSAIN

November 2018

Vacuum Kinetic Spray 법에 의한 광촉매 박막 제작

**Fabrication of Photocatalytic Thin Film by
Vacuum Kinetic Spray Method**

지도교수 천두만

이논문을 공학석사 학위 논문으로 제출함

2018 년 11 월

울산대학교 대학원

울산대학교 기계공학부

SADDAM HOSSAIN

Fabrication of Photocatalytic Thin Film by Vacuum Kinetic Spray Method

A Thesis

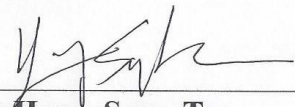
Submitted to the School of Mechanical Engineering and the Graduate School of
University of Ulsan, Republic of Korea in partial fulfillment of the requirements
for the degree of Master of Science in Mechanical Engineering

By

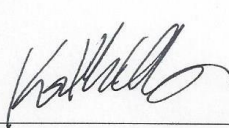
SADDAM HOSSAIN

November' 2018

**This certifies that the thesis of
SADDAM HOSSAIN is approved.**



Thesis Committee Chairman: Professor Hong, Sung-Tae



Thesis Committee Member: Professor Chung, Koo-Hyun



Thesis Committee Member: Professor Chun, Doo-Man

**The Graduate School
University of Ulsan
November 2018**

SADDAM HOSSAIN 의 공학석사 학위 논문을 인준함

심사위원장

홍성태

(인) 

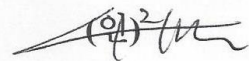
심사위원

정구현

(인) 

심사위원

천두만

(인) 

울산대학교 대학원

2018 년 11 월

ACKNOWLEDGEMENTS

Firstly, I am very thankful to almighty ALLAH for his blessings upon me in my whole life.

I would like to express my deepest gratitude to my advisor, Professor Doo-Man Chun, for his great support, guidance and providing me with an excellent atmosphere for doing research. I am a novice in conducting research. I can learn how to conduct research from him with his constant supervision. It is a great understatement to say that this work would not have been accomplished without his help. I thank him for the excellent effort and patience on me to train me up.

My sincere thanks to my colleagues of hybrid manufacturing technology laboratory, specially, Mohaned Mohammed Mahmoud Mohammed, who supported me a lot from the beginning of my journey. The outstanding friendly nature inside the laboratory helps me incredibly to do research.

Finally, I really would like to remember my late grandmother for her love and affection to me. My desire is to dedicate my master's degree to my late grandmother. I want to show my deepest love and respect to my wife, my uncle, my parents and other family members. They always encouraged me in any difficulties during my study and research. Moreover, I would like to thank all my friends, my teachers and my well-wishers.

Best regards,

Saddam Hossain

November 29' 2018

Ulsan, South Korea

ABSTRACT

Vacuum kinetic spray method is a dry particle deposition method, also known as the nano-particle deposition system (NPDS), to deposit metals and ceramics onto different substrates at room temperature without using any toxic chemicals. Nowadays, photocatalysis has been using as a green and clean process for renewable energy and environmental remediation. Various semiconductor materials like TiO_2 , WO_3 , Fe_2O_3 and so on are utilized in the photocatalysis field. Individual semiconductor materials can show poor photocatalytic efficiency because of high recombination effect of electron and holes. Therefore, no individual semiconductor can meet the required goal of photocatalysis. Consequently, the design of visible-light-driven semiconductor photocatalysts is a very important issue in terms of harvesting photon energy in the visible range. Recently, graphene has gained an enormous research interest due to its high specific surface area and electron mobility. In this study, NPDS is utilized to make WO_3 and its composite with (0-30) wt.% graphite thin films on polypropylene substrate.

To evaluate the photocatalytic activity of the fabricated thin films, degradation of methylene blue dye under illumination of light for 2 hours was observed. Degradation of the methylene blue dye was evaluated using absorbance values measured by UV/Vis spectroscopy at the wavelength of 665 nm. The results showed that the photocatalytic performance was significantly enhanced the graphite content is increased with WO_3 . The highest activity was observed for 15 wt.% graphite with WO_3 thin films. The photocatalytic reaction followed pseudo-first-order kinetics. The kinetic rate constant for graphene/ WO_3 with 15% graphite is 1.5 times higher than that of pristine WO_3 film. Repeatability determines the

feasibility of thin films in using real applications. Here, all the thin films showed good stability up to five cycles.

The deposited thin films were observed using field effect scanning electron microscopy (FE-SEM), X-ray diffraction (XRD) and Raman spectroscopy. FE-SEM shows that micro-sized graphite/ WO_3 particles are cracked into small pieces during deposition due to the high impact velocity by NPDS. X-ray diffraction showed the absence of any graphite peak in the composite thin film. Finally, the existence of graphene in the fabricated thin film was confirmed by Raman spectroscopy.

Finally, it is suggested that NPDS can be a suitable process for photocatalytic thin film fabrication at room temperature. The prepared thin films can be easily used for the photocatalytic applications.

Keywords: Vacuum kinetic spray, Nano-particle deposition system (NPDS), Thin film, Polypropylene, Photocatalysis, WO_3 , Graphene, Recombination effect, Methylene blue, Degradation.

CONTENTS

CHAPTER 1: INTRODUCTION.....	1
1.1 Introduction to Photocatalysis.....	2
1.2 Applications of Photocatalysis.....	4
1.3 Semiconductors in Photocatalysis.....	5
1.4 Strategies to improve photocatalytic activity.....	7
1.5 Graphene in Photocatalysis.....	8
1.6 Techniques for thin film fabrication	10
1.7 Objectives of this Research.....	11
CHAPTER 2: METHODOLOGY.....	12
2.1 Materials selection.....	13
2.2 Experimental setup.....	13
2.3 Summary of process parameters.....	15
2.4 Characterization of thin films.....	15
2.5 Photocatalytic activity analysis.....	16
CHAPTER 3: PHOTOCATALYTIC RESULTS.....	18
3.1 Absorbance value of MB dye.....	19
3.2 Degradation of methylene blue.....	20
3.3 Kinetics study.....	22
3.4 Repeatability of thin films.....	24
CHAPTER 4: THIN FILM CHARACTERIZATION.....	26
4.1 Optical images of thin films.....	27
4.2 Mass of thin films.....	27

4.3	Confocal Microscopy.....	28
4.4	FE-SEM.....	30
4.5	XRD.....	31
4.6	Raman Spectroscopy.....	33
CHAPTER 5: DISCUSSION.....		35
CHAPTER 6: CONCLUSION.....		38
ACKNOWLEDGEMENT.....		41
BIBLIOGRAPHY.....		42

LIST OF TABLES

Table. 1 Band gap of some common semiconductors	6
Table. 2 Graphene/semiconductor photocatalysts.....	9
Table. 3 Process parameters for graphite and WO ₃ deposition on PP substrate.....	15

LIST OF FIGURES

Figure 1.	Principle of photocatalysis	3
Figure 2.	Applications of photocatalysis	4
Figure 3.	Techniques to improve photocatalytic activity	8
Figure 4.	Objectives of this research.....	11
Figure 5.	Schematic for the vacuum kinetic spray method.....	14
Figure 6.	Photocatalytic set-up for MB dye degradation.....	17
Figure 7.	Flowchart for photocatalytic activity analysis.....	17
Figure 8.	Absorbance of the MB dye after 2 hours of light illumination.....	19
Figure 9.	Absorbance vs. wavelength as a function of irradiation of time for MB dye degradation (a) WO_3 film and (b) WO_3 film with 15 wt.% graphite.....	20
Figure 10.	Degradation of MB dye for different wt.% of graphite with WO_3 photocatalyst under halogen light irradiation for 2 hours.....	21
Figure 11.	Degradation of MB dye for WO_3 powders and films.....	22
Figure 12.	Kinetic analysis of the WO_3 film and graphene/ WO_3 film with 15 wt.% graphite for MB dye degradation.....	23
Figure 13.	MB dye degradation rate of pure WO_3 film and 15% graphite/ WO_3 film.....	24
Figure 14.	Repeatability of degradation of graphene/ WO_3 film with 15 wt.% graphite.....	25
Figure 15.	Thin films of (a) WO_3 and (b) graphene/ WO_3 film with 15 wt.% graphite by NPDS; before and after photocatalytic experiment.....	27
Figure 16.	Mass per unit area of thin films.	28

Figure 17. Confocal microscopy images for (a) WO ₃ film and (b) graphene/WO ₃ film with 15 wt.% graphite.....	29
Figure 18. Thickness of the as-deposited thin films.....	29
Figure 19. FE-SEM images of (a) WO ₃ powders, and (b) graphite powders.....	30
Figure 20. FE-SEM images of thin films (a) & (b) WO ₃ film, and (c) & (d) graphene/WO ₃ film with 15 wt.% graphite.....	31
Figure 21. XRD patterns of (a) graphite powders, (b) WO ₃ powders, (c) PP, (d) WO ₃ film, and (e) graphene/WO ₃ film with 15 wt.% graphite.....	32
Figure 22. Raman spectra of graphite powders, WO ₃ powders, PP, WO ₃ film, and graphene/WO ₃ film with 15 wt.% graphite.....	34

LIST OF ABBREVIATIONS

Sl. No.	Short Form	Full Form
1	NPDS	Nano-particle deposition system
2	SoD	Stand-off distance
3	VB	Valence band
4	CB	Conduction band
5	UV -Vis	Ultraviolet -Visible
6	DSSC	Dye sensitized solar cells
7	WO ₃	Tungsten oxide
8	PP	Polypropylene
9	MB	Methylene blue
10	DI	Deionized
11	FESEM	Field emission scanning electron microscopy
12	XRD	X-ray diffraction

CHAPTER 1

INTRODUCTION

1.1 Introduction to Photocatalysis

Water contamination with different organic dyes is a very acute problem in today's world. The toxic chemicals throwing into water from the industries impart adverse effects on humans and environment. Therefore, proper treatment of wastewater containing harmful dyes before discharging to the environment is required to protect the environment. There are some conventional processes to remove waste from water. But, they are not effective enough to purify the water fully. Furthermore, these types of processes generate secondary pollutants that need more purification. They are very slow, require more cost and some processes need very high temperature [1–4]. Consequently, a very promising technique is a crucial need for the complete purification of wastewater. Recently, semiconductor photocatalysis has been an immense interest in the application of solar energy and environmental remediation. Researchers are looking forward to semiconductor process because of some important features: i) photocatalysis is a sustainable process because of using the clean and safe energy from sun, ii) it is economically viable and environmentally friendly process because it does not produce any secondary hazardous pollutants, iii) it is a room temperature and pressure, and iv) it has low cost [5]. Semiconductors due to their suitable energy band gap matching with the solar energy has been a great interest in photocatalysis field. Photocatalysis is a catalytic process which accelerate the chemical reaction rate utilizing renewable solar energy. The chemical process is usually oxidation/reduction reaction where semiconductors can make electrons and holes in the presence of light. An ideal photocatalytic material should have good photostability, able to absorb ultraviolet (UV) or visible (Vis) wavelengths of light, chemically or biologically inert, non-toxic and cheap. Semiconductor photocatalysts being irradiated under UV or Vis light form electrons (e^-) and holes

CHAPTER 1: INTRODUCTION

(h^+). To make photogenerated electrons and holes, the light energy ($h\nu$) should be greater than the band gap energy of semiconductors (E_g), i.e; $h\nu \geq E_g$. The electrons from valence band (VB) are excited to conduction band (CB) with breaking the band gap energy barrier shown in **Fig. 1**. The photogenerated electrons can react with oxygen dissolved in water to reduce it oxide radical $\cdot O_2^-$ and then OH. Radicals. On the other hand, the photogenerated holes can also oxidize water to make OH. Radicals. These hydroxyl radicals then degrade the organic dye to make harmless H_2O and CO_2 [6–8]. The chemical reactions with semiconductor photocatalysis to degrade organic dyes are as follows:

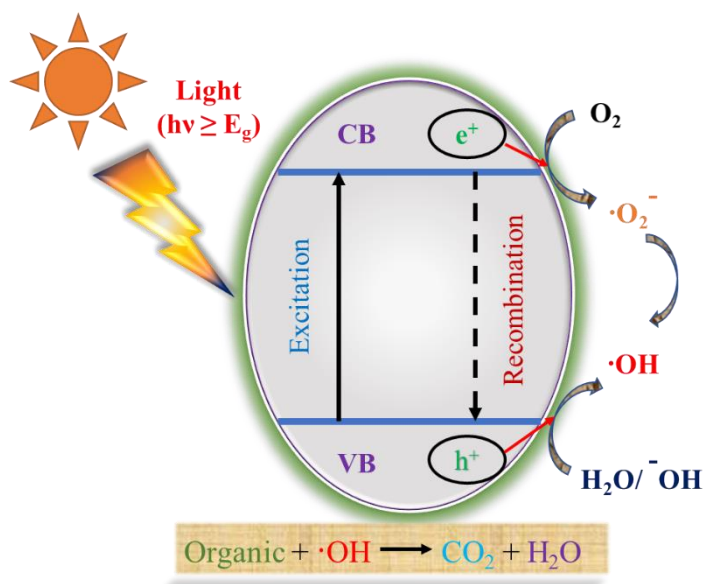
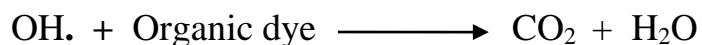
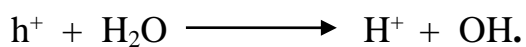
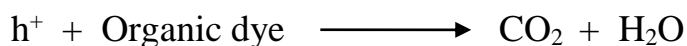
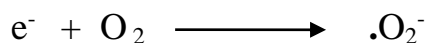
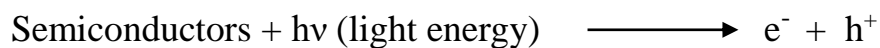


Fig. 1. Principle of photocatalysis.

In the photocatalytic process, there is an increasing chance to recombine the photogenerated electron in the CB if the oxygen reduction and the oxidation of dye do not advance simultaneously. Therefore, it is very important to suppress the recombination rate of photogenerated electrons and holes for the semiconductor photocatalysis research.

1.2 Applications of Photocatalysis

Photocatalysis with semiconductor materials is one of the promising research topics due to its numerous uses in various fields as wastewater treatment, H_2 production, artificial photosynthesis (CO_2 reduction), removal of toxic gases from air, and dye sensitized solar cells (DSSC) [9–13]. The application of photocatalysis are shown in **Fig. 2**.

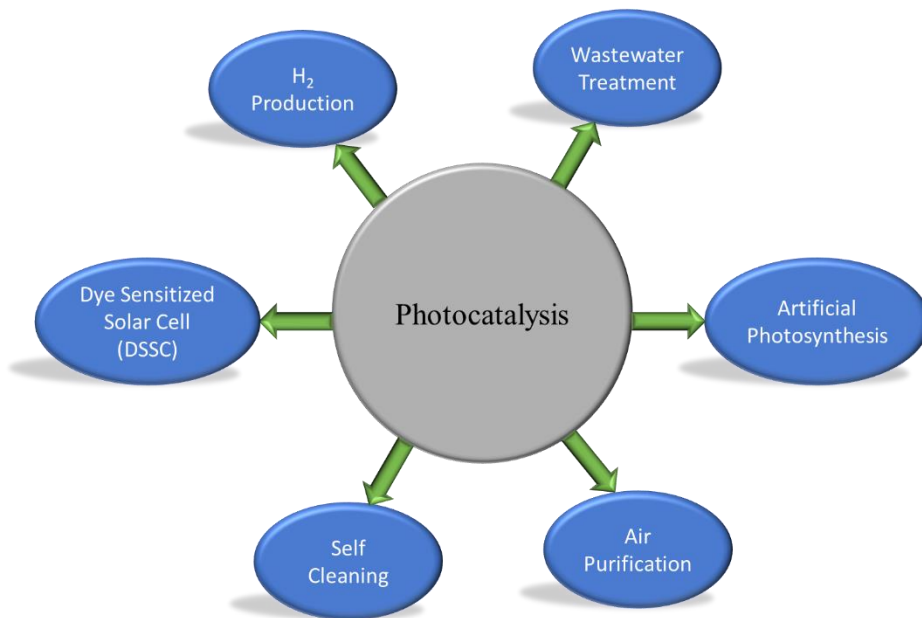


Fig. 2. Applications of photocatalysis.

1.3 Semiconductors in Photocatalysis

Photocatalysis as a clean and green process has gained much attention as a promising technique for environmental remediation. There are many semiconductors that are using in the photocatalytic activity analysis with solar light illumination. Some semiconductors can utilize only the UV portion of sunlight because of their band gap energy. **Table 1** shows the band gap energies of some common semiconductor materials. By the work of Fujishima and Honda in 1972 [14] with photoelectrochemical hydrogen and oxygen production using (titanium oxide) TiO_2 electrode with UV light illumination, there has been an increasingly growing interest with photocatalysis process. Since then TiO_2 is the most studied photocatalytic semiconductor material due to its high oxidation ability, high chemical stability, nontoxicity, and low cost. Three TiO_2 crystal forms of anatase, rutile, and brookite are available in nature. Rutile form is mostly stable, but the organic degradation efficiency is higher for anatase than rutile in some cases. The brookite is the less studied [9]. However, TiO_2 is suitable in the UV region (the band edge for TiO_2 is near 387 nm) because of its high band gap energy (~ 3.2 eV). It can absorb only $\sim 5\%$ energy irradiated from sun [15]. So, it cannot utilize the largest part of solar energy that is the visible energy and hence limits the solar conversion efficiency. Hematite or $\alpha\text{-Fe}_2\text{O}_3$ has a low band gap of about 2.2 eV and can catch 40% of the photonic energy irradiated from the sun which is in the visible range. Also, it is a nontoxic, chemically stable, abundance in nature and low cost semiconductor [16]. Nevertheless, the photocatalytic performance of Fe_2O_3 is still poor due to high recombination of electron holes, poor mobility of charge carriers ($< 0.2 \text{ cm}^2 \cdot \text{V}^{-1} \cdot \text{s}^{-1}$), the short diffusion length of the holes (2-4 nm), and short lifetime of the photogenerated charge carriers (< 10 ps) [17]. In addition, tungsten oxide (WO_3), an environmentally friendly n-type semiconductor, has

proven to be a good photocatalyst owing to its light absorption in the visible range. WO_3 has also a suitable band gap (2.4-2.8) with some unique properties i.e., nontoxicity, stability, resistance to photo-corrosion, and high oxidation power [18–20]. But, WO_3 also exhibits poor activity as the reduction of oxygen is not easily initiated due to the unfavorable conduction band position and the tendency of electron-hole recombination. The photogenerated electrons in the CB of WO_3 cannot react with oxygen molecules efficiently to reduce oxygen into oxide radicals because of the CB level is more positive than the potential for the single-electron reduction of oxygen. So, the photoinduced electron gather on the surface of WO_3 which acts as a recombination center and hence, WO_3 can show poor photocatalytic activity [21–23]. Other metal oxides for example, ZnO , ZnS , MoS_2 , ZnWO_4 , CdS , CuO , $\text{g-C}_3\text{N}_4$, SnO_2 , $\text{Sr}_2\text{Ta}_2\text{O}_7$, etc. have been using in the field of semiconductor photocatalysis [24–32]. As individual semiconductors has their own disadvantages, no semiconductor can meet the required goal of photocatalysis.

Table 1 Band gap of some common semiconductors.

Semiconductor	Band gap (eV)
Titanium oxide (TiO_2)	~3.2
Tungsten oxide (WO_3)	~2.8
Iron oxide (Fe_2O_3)	~2.2
Zinc oxide (ZnO)	~3.4
Zinc sulphide (ZnS)	~3.6
Cadmium sulphide (CdS)	~2.4
Lead sulphide (PbS)	~0.28
Tin oxide (SnO_2)	~3.5
Copper(I) oxide (Cu_2O)	~2.0
Zirconium oxide (ZrO_2)	~3.8
Molybdenum disulfide (MoS_2)	~1.75
Bismuth vanadate (BiVO_4)	~2.3
Graphitic carbon nitride ($\text{g-C}_3\text{N}_4$)	~2.7
Bismuth tungstate (Bi_2WO_6)	~2.8

1.4 Strategies to improve photocatalytic activity

The photoinduced electrons and holes for a single semiconductor can go a quick recombination and consequently, decrease the photocatalytic activity. There has been many strategies adopted for the improvement of the photocatalytic process for individual photocatalyst. Surface modifications, doping with other materials, composite formation, and formation of multilayers are the most common strategies shown in **Fig. 3** to improve the photocatalytic performance [33]. Doping of noble metals with semiconductors are found to be an effective means to increase the photo-efficiency [34–36]. Although noble metals are effective, the high cost of these metals limits their practical use [37]. Another important route to enhance photocatalytic activity is composite formation of metal oxides/metal oxides. In this particular strategy, semiconductors with other semiconductors are mixing together with different ratios to find out the optimal level where the composite shows highest performance. The light absorption region can be increased by tuning the band gap and the recombination may be suppressed by the efficient charge transfer by the two or more composite mixing and hence, improved photocatalytic performance. TiO_2/WO_3 , $\text{TiO}_2/\text{Fe}_2\text{O}_3$, $\text{WO}_3/\text{Fe}_2\text{O}_3$, $\text{TiO}_2/\text{MoS}_2$, $\text{CdS}/\text{Ni}(\text{OH})_2$ are some of the examples of composite formation for the improvement of photocatalytic performance [37–41]. Recently, improvement of semiconductor photocatalysis with carbonaceous materials, such as carbon nanotubes (CNTs) and graphene having large specific surface area and high electron mobility is an efficient strategy [26,42].

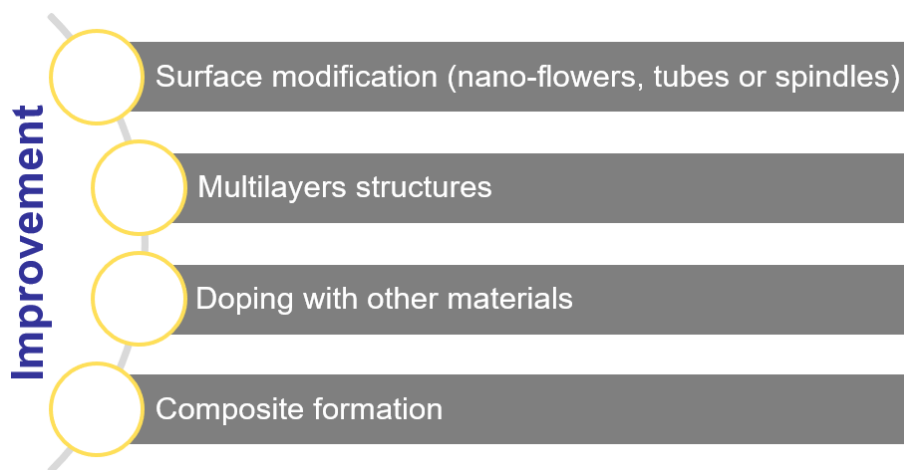


Fig. 3. Techniques to improve photocatalytic activity.

1.5 Graphene in Photocatalysis

Graphene is an exciting material for its unique properties and enormous application areas. Graphene has unique 2D honeycomb lattice structure with single layer of sp^2 bonded carbon atoms. Graphene has been widely used in different application areas due to its large theoretical specific surface area ($2630 \text{ m}^2\text{g}^{-1}$) and a π -conjugation structure that exhibits excellent electron mobility ($200,000 \text{ cm}^2\text{V}^{-1}\text{s}^{-1}$) [43]. Also, it has high adsorption capacity and electrical conductivity. Recently, there has been an exciting progress in the development of graphene/semiconductor composites photocatalyst among different applications of graphene because of its unique properties. Most of the photocatalysts that are using nowadays cannot utilize visible light and hence, very poor photocatalytic efficiency under visible light. So, a facile design technique has to be obtained to develop efficient photocatalysts for the practical applications. It is reported that semiconductors with graphene is a very good strategy to improve the photocatalytic performance and stabilities. Zhu et al. [44] reported that RGO- WO_3 composites are very effective for degradation of sulfamethoxazole by a one-step hydrothermal method. Zhang et al.

CHAPTER 1: INTRODUCTION

[45] observed a significant enhancement in the degradation of methylene blue with P25-graphene over the bare P25 and P25-CNTs using a facile one-step hydrothermal method. **Table 2** shows some graphene based photocatalysts for the improvement of the photocatalytic performance. Together with semiconductor materials, graphene can extend the light absorption domain and, as a result, yield improvement in the activity of photocatalytic dye degradation, which can be achieved as graphene acts as a support for the electron.

Table 2 Graphene/semiconductor photocatalysts.

Materials	Photocatalytic property	Ref.
Hematite/RGO	the enhanced activity toward oxygen evolution	[17]
WO ₃ -RGO	Significant enhancement in photodegradation of MB	[20]
Graphene-WO ₃ Nanorod	96% of RhB removal after 2h of visible-light	[21]
ZnO/Graphene	2 and 3.5 times by graphene/ZnO under Vis and UV	[24]
MoS ₂ /Graphene	Efficient H ₂ Evolution under Visible Light Irradiation	[26]
ZnWO ₄ /Graphene	High efficiency for degradation of MB	[27]
CdS/graphene	about 4.87 times higher than pure CdS nanoparticles	[28]
TiO ₂ nanoparticles on graphene	enhanced photocatalytic degradation of rhodamine 6G	[46]
WO ₃ /graphene	MB degradation under visible-light	[47]
WO ₃ on carbon paper	89% of the RB decomposed after 11 h visible light	[48]
Mesoporous WO ₃ - graphene	degradation of Methylene Blue dye under visible light illumination	[49]
TiO ₂ /RGO	the best photocatalytic activity observed for the composite of 2.0 wt % RGO	[50]
α -Fe ₂ O ₃ /Graphene	98% of Rhodamine (RhB) decomposed	[51]

1.6 Techniques for thin film fabrication

Previously, photocatalysts in powder form were mainly used to carry out research in photocatalysis. However, it is reported that there are some problems with powder forms. Usually, the particles are agglomerated together which lead to decrease in photocatalytic performance. Also, the removal of suspended particles from the solution is very difficult; hence, particles are usually lost during recovery which also decrease the activity. Furthermore, the recovery process is costly because it needs more purification steps [52–54]. It is possible to overcome these limitations by immobilizing catalyst particles as thin films on various substrates as support. There are many techniques to make thin films for the application in photocatalysis. Some techniques including sol-gel, hydrothermal, and chemical vapor deposition (CVD), spray pyrolysis, thermal vacuum evaporation technique have been used to make solid films on substrates [55–63]. However, some of these methods are not environmentally friendly, need toxic chemicals, high process temperature, longer process times and also expensive. To solve these problems, a facile dry particle deposition is used at room temperature.

In this research, we report a room temperature vacuum kinetic spray method, also known as nano-particle deposition system (NPDS) to import thin films on polypropylene substrate. The NPDS is one of the dry spray deposition techniques to coat metals and ceramics at room temperature and low vacuum conditions without any toxic chemicals. It is reported that NPDS is capable of depositing various types of metal and ceramic particles including TiO_2 , Al_2O_3 , Ni, and Sn onto different substrates (Cu, Al, polymers) [64–68]. Recently, few-layer graphene flake structures were formed from microscale graphite particles, and their deposition behaviors on different substrates were studied using the NPDS method [69,70].

1.7 Objectives of this Research

In this study, graphite and WO_3 powders with different graphite contents (0 - 30 wt.%) were deposited on polypropylene (PP) by NPDS. The photocatalytic activity of thin films by methylene blue (MB) dye degradation under irradiation of light for 2 hours was observed with UV-Vis spectroscopy. The reusability of thin films was assessed, and the kinetic behavior of the reaction was studied. The thin films were characterized by X-ray diffraction (XRD), confocal microscopy, field emission scanning electron microscopy (FE-SEM), and Raman spectroscopy.

The objectives of this research are:

1. To make thin films of graphite and WO_3 particles by environmentally friendly vacuum kinetic spray method.
2. To characterize the thin films.
3. To improve the photocatalytic performance.

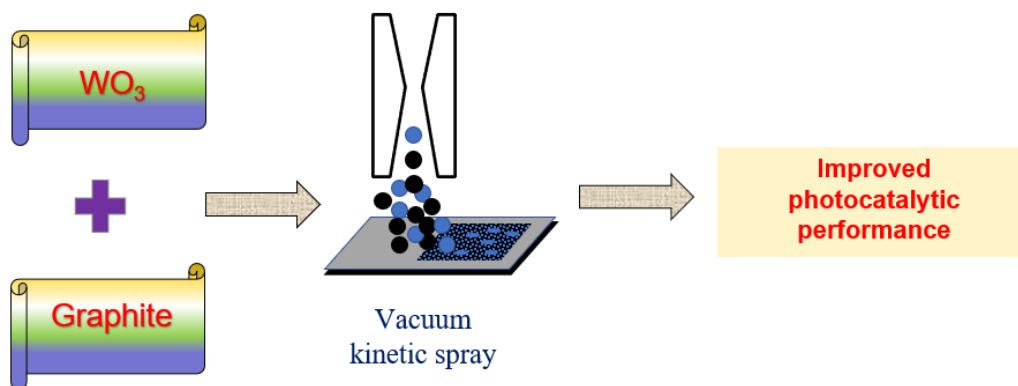


Fig. 4. Objectives of this research.

CHAPTER 2

METHODOLOGY

2.1 Materials selection

Micro-sized WO_3 powder ($\leq 20\mu\text{m}$, 272785, Sigma-Aldrich, Korea) and micro-sized graphite powder (MGF 10 995A, Samjung CNG, Korea) were used as purchased. Polypropylene (PP) plate ($5\text{ mm} \times 5\text{ mm} \times 5\text{ mm}$) is used to support the thin film. Methylene blue (5578-4125, Daejung, Korea) was used as an organic material to observe the degradation.

2.2 Experimental setup

Firstly, micro-sized WO_3 powders and graphite powders weighted together as the ratio of 100:0, 95:5, 90:10, 85:15, 80:20, and 70:30 by the precise measurement with weight measuring machine. The weighted powders were then mechanically mixed via a ball mill machine with 4h and 600 rpm. Every time prior to deposition, the powders were dried for 2h with 80° temperature to remove the moisture. After that, graphite and WO_3 powders with different graphite contents were deposited on PP plates by kinetic spraying. The NPDS consists of a compressor to supply compressed air, a cylinder-piston type powder feeder, a vacuum pump, a nozzle, and a controller, as shown in **Fig. 5**. The powders stored in the cylinder come to the brush chamber section when the piston moved up. The high rotational speed of brush drives the powders into the main stream of pressurized carrier gas coming from air compressor. The pressurized carrier gas can easily carry the powders to a converging nozzle where it sprays the powders onto the substrate with high speed

CHAPTER 2: METHODOLOGY

utilizing the pressure difference between compressed air and vacuum. The powders utilizing the kinetic energy can easily be fragmented and deposited on PP. A suitable SoD, i.e. the distance between the substrate and nozzle is maintained for this research because the deposition behavior also depends on SoD. The thin films were prepared within very short time. The prepared films were immediately cleaned ultrasonically using DI water for 5 minutes, followed by air cleaning. The films were then kept in a clean place to dry completely prior to use for the photocatalytic MB dye degradation analysis.

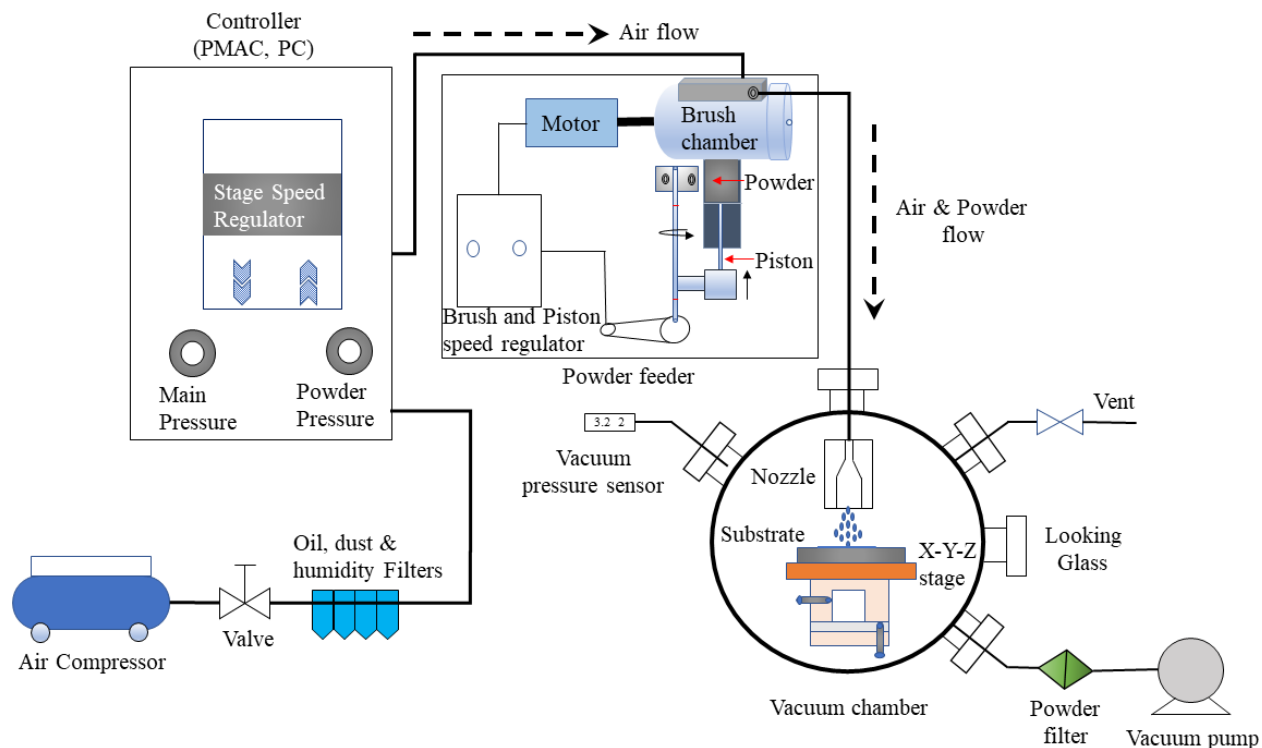


Fig. 5. Schematic for the vacuum kinetic spray method.

2.3 Summary of process parameters

Process parameters are very important depositing with vacuum kinetic spray method. Any parameter has not been changed during the whole experiment. Complete constancy of parameters was maintained for graphite and WO_3 deposition. **Table 3** gives the detail information about process parameter.

Table 3 Process parameters for graphite and WO_3 deposition on PP substrate.

Parameters	Value
Air Pressure (MPa)	0.3
Chamber pressure (MPa)	0.041 ~ 0.043
Distance between substrate and nozzle (mm)	2.0
Stage speed (mm/s)	0.3
Piston speed (mm/s)	0.26
Piston bore diameter (mm)	14
Brush speed (rpm)	12000
Deposition area (cm × cm)	4 × 4
Nozzle dimension (mm × mm)	5 × 0.4

2.4 Characterization of thin films

The morphology of the graphite powders, WO_3 powders, and deposited thin film was observed by FE-SEM (JSM-6500F, Jeol, Japan) with an operating voltage of 10 kV. A confocal Raman spectrometer (alpha 300R, WITec, Germany) was utilized to obtain detailed information about structures of powders and deposited thin films using a 532 nm wavelength and laser excitation source at 1 mW. XRD (Ultra 4, Rigaku, Japan) was used to collect diffraction patterns from graphite

powders, WO₃ powders, PP plate, and deposited thin films from a 10 to 60° range of 2 thetas with a CuK α source of radiation. The surface was observed, and film thickness was calculated using 3D laser scanning confocal microscopy (VK-X200 series, Keyence, Japan).

2.5 Photocatalytic activity analysis

The photocatalytic performance of pure WO₃ film and its various composite with graphite particles were analyzed by degrading 100 ml of 5 ppm methylene blue (MB) solution. Pure MB solid particles were measured and dissolved in deionized (DI) water to make 1000 ppm and 5 ppm of MB dye was prepared from 1000 ppm. 100 ml of 5 ppm was then taken into a beaker where the coated substrate was placed on the bottom of the beaker to irradiate 100 W halogen light. The films on polypropylene were exposed to the visible light source continuously for 2 hours. The distance from the light source to the substrate was kept 26 cm. The schematic diagram for this system is shown in **Fig. 6**. A 3ml of aliquot was collected after 2h of light irradiation and a UV-Vis spectrometer (Optizen POP, Mecasys, Korea) was used to measure the absorbance value of MB dye at 665 nm. The following equation (1) is used to calculate the % degradation of MB dye.

$$\% \text{ Degradation} = \frac{A_0 - A_t}{A_0} \quad (1)$$

where A_0 and A_t are the absorbance values before and after a 2 h exposure to light, respectively. After every 20 minutes, 3 ml solution was taken to realize the kinetic behavior of MB dye degradation. The samples were reused five times after

cleaning with H_2O_2 to show the recyclability. The total work in this paper is described briefly with the flow chart in **Fig. 7**.

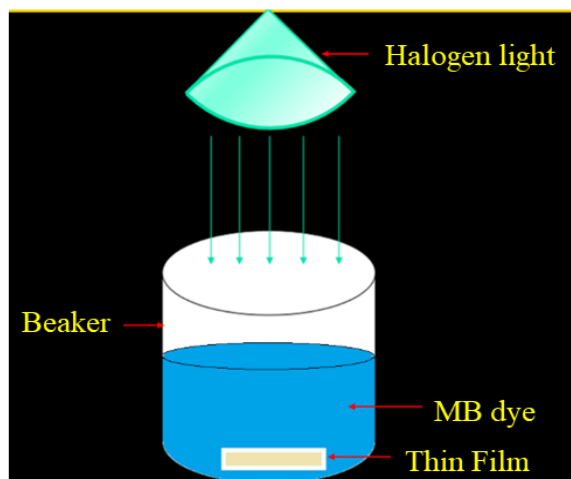


Fig. 6. Photocatalytic set-up for MB dye degradation.

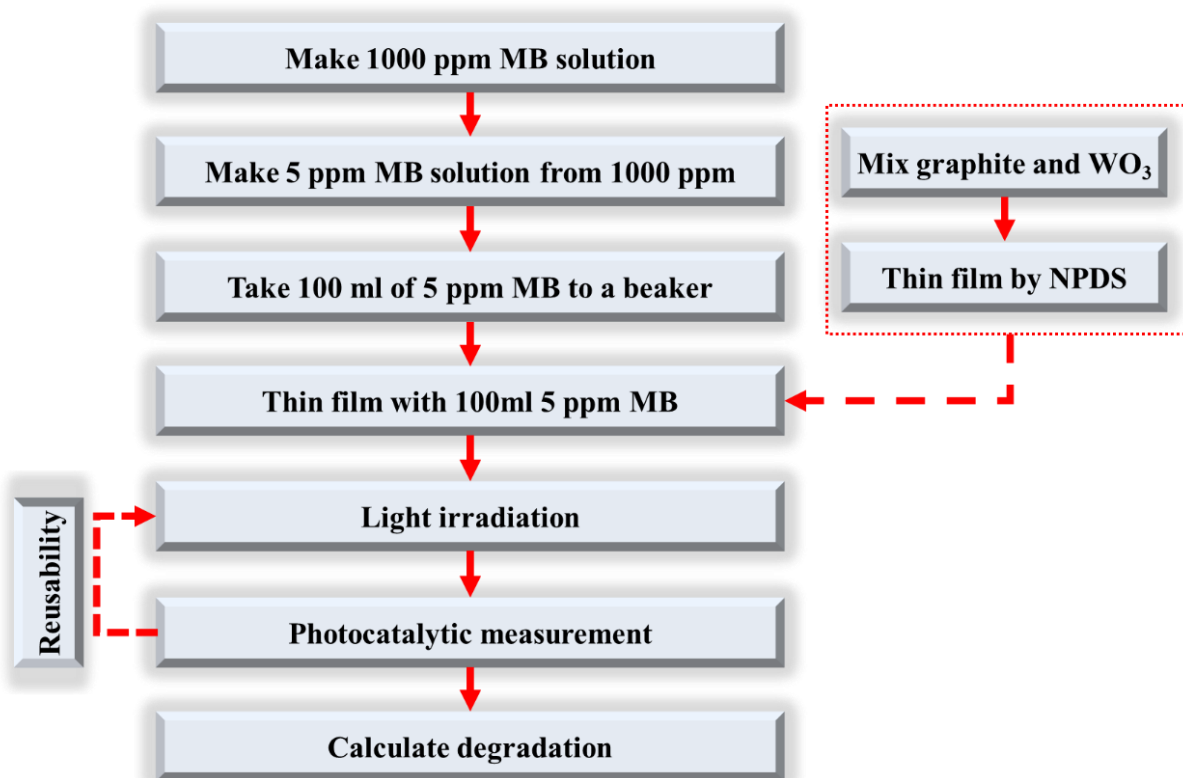


Fig. 7. Flowchart for photocatalytic activity analysis.

CHAPTER 3

PHOTOCATALYTIC RESULTS

3.1 Absorbance value of MB dye

Methylene blue solution was prepared to investigate the photocatalytic degradation with series of thin films of graphite and WO_3 prepared by dry particle deposition method. Experimental results of the degradation of MB in the presence of visible light were depicted in **Fig. 8**. Six types of samples (pure WO_3 film, 5, 10, 15, 20, 30 wt.% graphite + WO_3 film) were prepared by NPDS and then used as photocatalyst into MB dye to observe degradation after 2h continuous visible light irradiation via 100W halogen light. UV-Vis spectrometer was used to measure the absorbance value from 400-800 nm after the light illumination to realize the photocatalytic efficiency. The absorbance value of pure MB was also measured before light to compare with the absorbance value after light irradiation. **Fig. 9** shows the time dependent absorbance behavior. For composite thin film, the degradation is more than the pure WO_3 film.

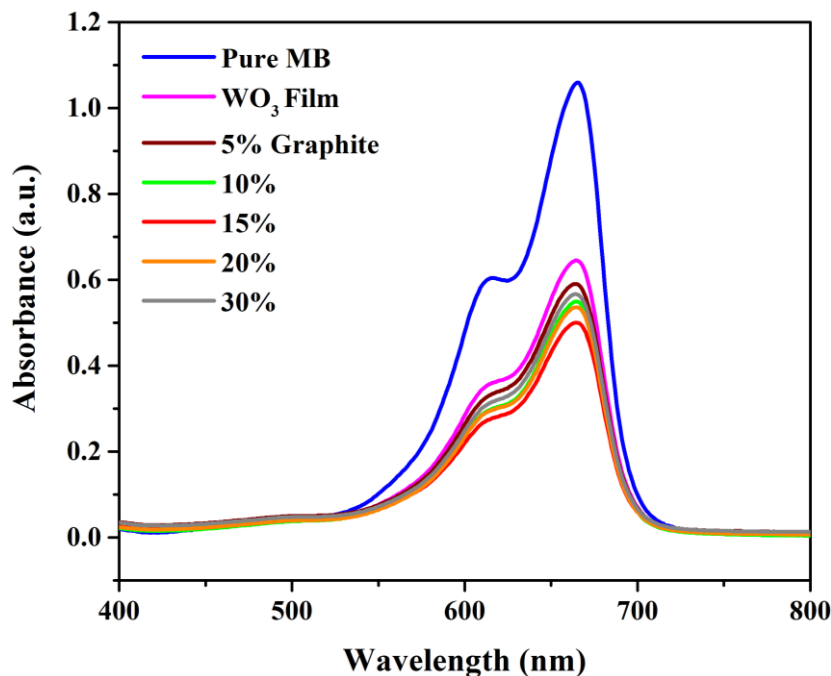


Fig. 8. Absorbance of the MB dye after 2 hours of light illumination.

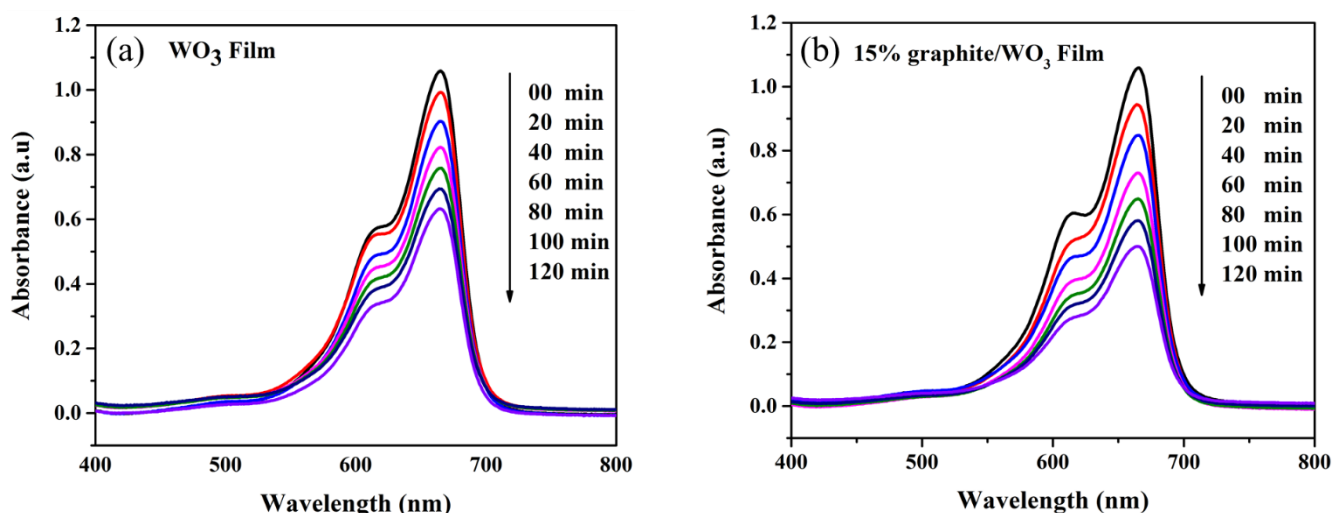


Fig. 9. Absorbance vs. wavelength as a function of irradiation of time for MB dye degradation (a) WO_3 film and (b) WO_3 film with 15 wt.% graphite.

3.2 Degradation of methylene blue

After measuring the absorbance value, the peak value for MB dye at 665 nm wavelength was used to calculate the degradation percentage. The degradation value was depicted in **Fig. 10**. All the thin films fabricated by NPDS on PP exhibited considerable amount of photocatalytic degradation for MB dye under halogen light irradiation. Initially, pristine WO_3 films were exposed to light source for 2 hours. The MB dye was degraded about 39% for pure WO_3 thin films. Then, all the composite thin films of WO_3 with graphite content were utilized to show the improved photocatalytic activity. The photocatalytic performance was increased when graphite wt.% was increased from 0% to 15%. Five thin films for each composite were used to observe the photocatalytic activity of the MB dye as well as film-dependent behavior. All five samples for each composite, with only a small variation in degradation, showed consistent results. It was clear that all composite

thin films with varying graphite contents exhibited an enhancement in degradation of MB dye compared to pure WO_3 thin films, demonstrating that the highest degradation occurred with the composite thin film containing 15 wt.% graphite powders. However, at a certain amount of graphene, it is obvious that the photocatalytic performance is reduced from the highest photocatalytic activity. In our research, the highest activity of MB dye degradation is for 15 wt.% graphite/ WO_3 . After the highest activity, the photocatalytic activity is then started to decrease when added graphite is more than 15 wt.%. For 20% and 30% graphite with WO_3 films, the photocatalytic efficiency is decreasing but it is still higher than that of pure WO_3 film. The reasons why the photocatalytic performance is increasing and decreasing mode is discussed in the discussion section.

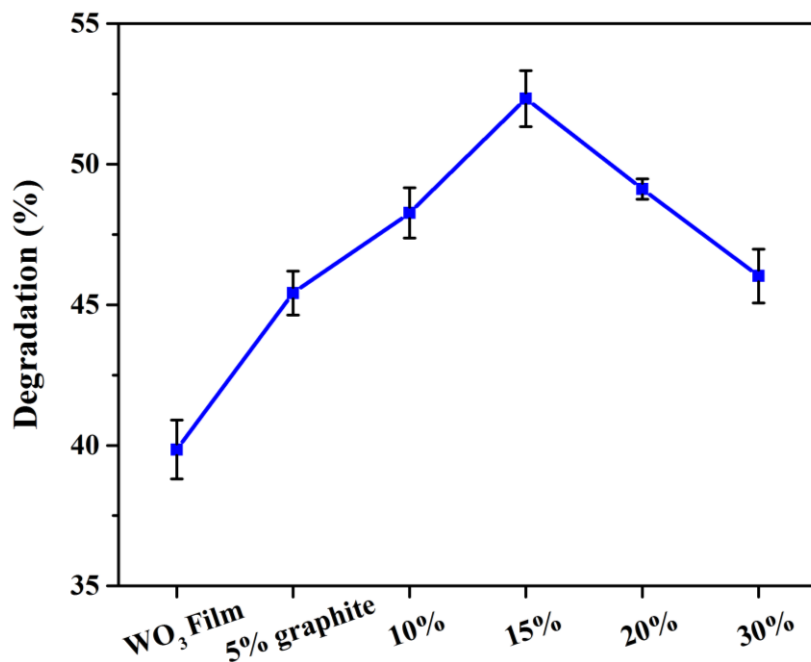


Fig. 10. Degradation of MB dye for different wt.% of graphite with WO_3 photocatalyst under halogen light irradiation for 2 hours.

The degradation of MB dye with WO_3 powder photocatalyst were also analyzed to compare with the WO_3 thin films which is shown in **Fig. 11**. The thin films showed higher degradation efficiency than the powder catalyst because of higher exposed area of thin films to light than powders.

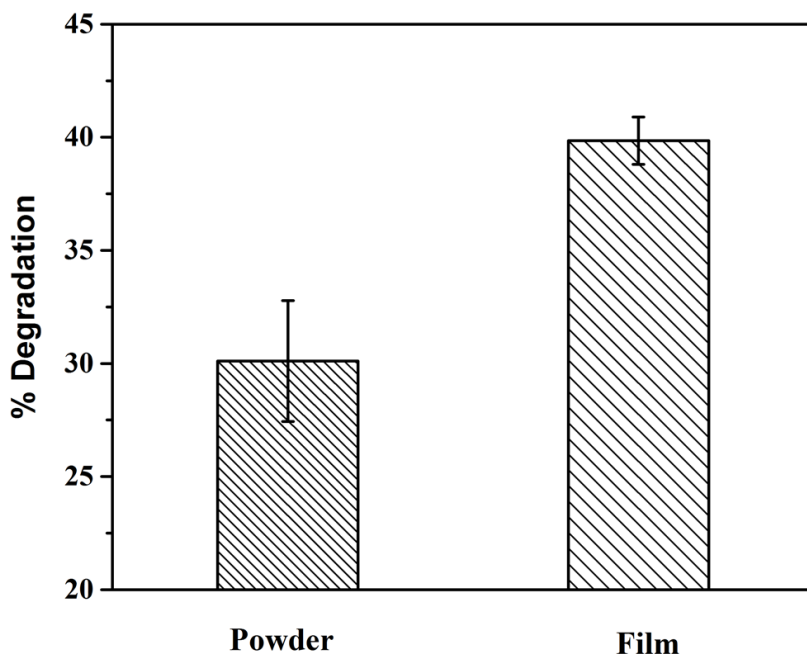


Fig. 11. Degradation of MB dye for WO_3 powders and films.

3.3 Kinetics study

The study of kinetics is very important to realize the reaction behavior of photocatalytic dye degradation. As displayed in **Fig. 12** the curves for pure WO_3 film and WO_3 thin film with 15% graphite are fitted linearly to examine the type of photo-chemical reaction by plotting the natural log of (A_0/A_t) vs. time. In this study, to measure the kinetics of pristine WO_3 film and its composite with 15% graphite, 3 ml aliquot was collected from 5 ppm, 100ml MB dye after every 20 minutes for 2 hours. The absorbance of methylene blue was measured at the wavelength at 665

nm. The slope of the fit represents a first-order reaction rate of the MB solution. The photocatalytic reactions for both WO_3 film and 15% graphite- WO_3 showed pseudo-first-order kinetics because they followed a straight line. Equation (2) was used to calculate the reaction rate constant.

$$\ln (A_0/A_t) = kt \quad (2)$$

where A_0 and A_t are the initial concentration and final concentration at time t , respectively, and k is the reaction rate constant. Importantly, it can be clearly seen from **Fig. 13** that the reaction rate of 15% graphite/ WO_3 thin film is higher than that of pure WO_3 film. So, the of composite thin films of WO_3 with graphite show good photocatalytic performance than its counterpart with WO_3 films. The reaction rates (k value) for pure WO_3 film and 15% graphite/ WO_3 film are $4.23 \times 10^{-3} \text{ min}^{-1}$ and $6.12 \times 10^{-3} \text{ min}^{-1}$, respectively. The photocatalytic improvement for 15% graphite/ WO_3 thin film as from reaction rate is 1.5 times higher than that of pure WO_3 film.

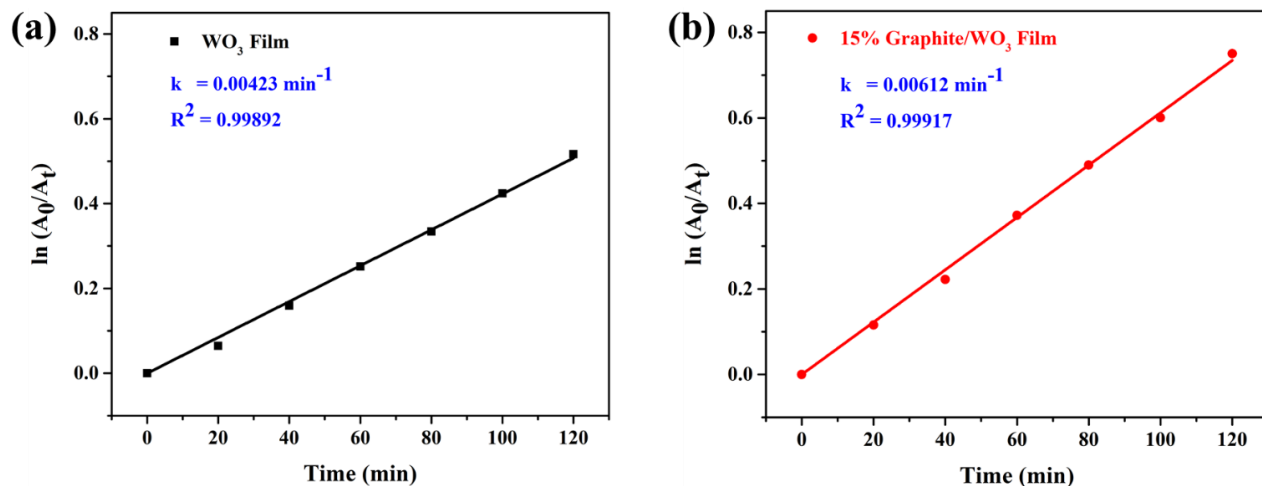


Fig. 12. Kinetic analysis of (a) WO_3 film, and (b) graphene/ WO_3 film with 15 wt.% graphite for MB dye degradation.

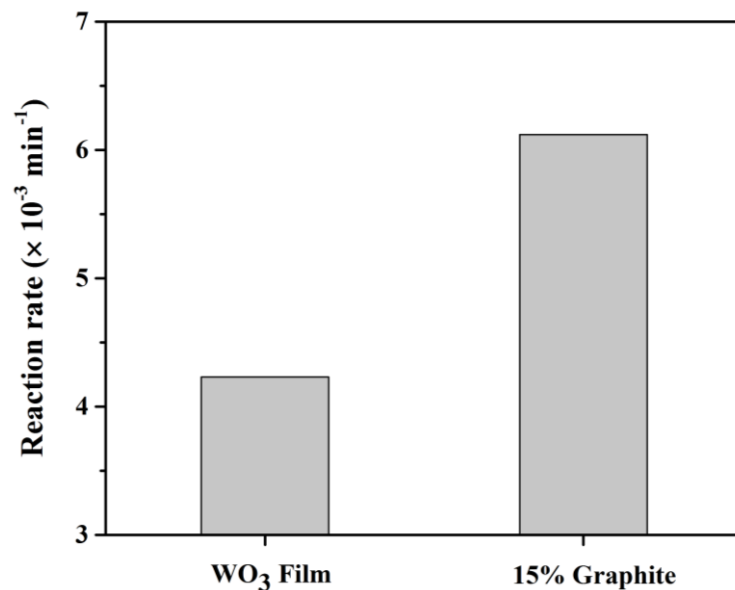


Fig. 13. MB dye degradation rate of MB for pure WO₃ film and 15% graphite/WO₃ film.

3.4 Repeatability of thin films

Fig. 14 illustrates the stability of 15% graphite/WO₃ upon reuse. The efficacy of 15% graphite-WO₃ film was analyzed five times to investigate the durability during reuse. The films were washed with H₂O₂ followed by cleaning with DI water and then dried for further use. The results evidently demonstrated that the films prepared by NPDS can effectively be reused while maintaining high photocatalytic efficiency as fresh thin films, indicating that photocatalyst is stable and reusable. However, a small deterioration can be obtained due to the washing process and/or environmental changes. It can be said that NPDS is a good thin film fabricating process for the application of photocatalysis.

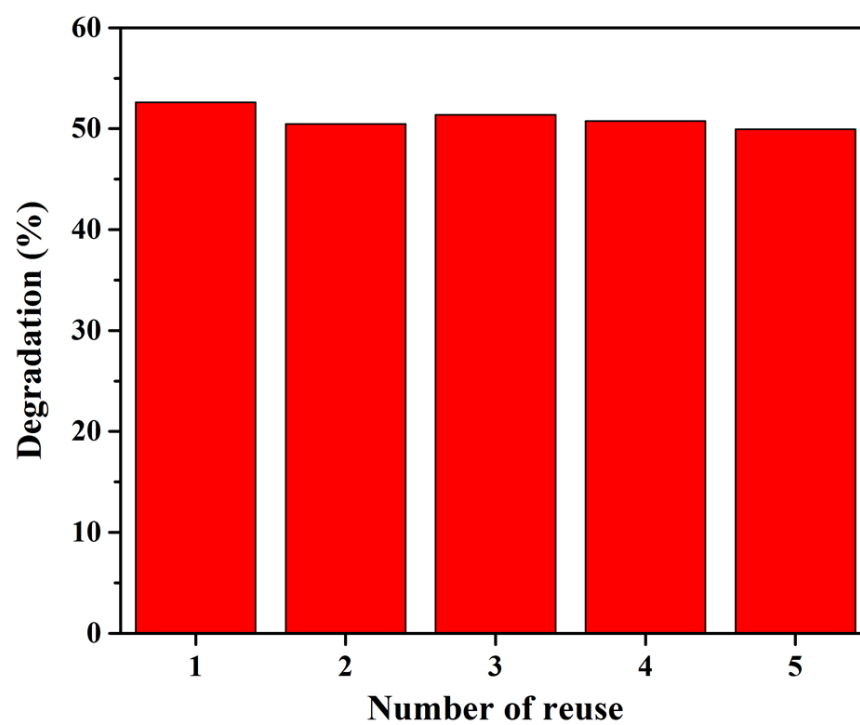


Fig. 14. Repeatability of degradation of graphene/WO₃ film with 15 wt.% graphite

CHAPTER 4

THIN FILM CHARACTERIZATION

4.1 Optical images of thin films

The thin films of pure WO_3 and composite with graphite particles were prepared by NPDS within very short process time. To support thin films, cheap PP plate was used. After fabrication of thin films, they were washed and dried to use for the photocatalytic analysis. The colour of thin films was changed to blue because the coating surface adsorbs the molecules of MB dye. **Fig. 15** illustrates the solid thin films for pure WO_3 and its composite with 15% graphite after and before photocatalytic analysis.

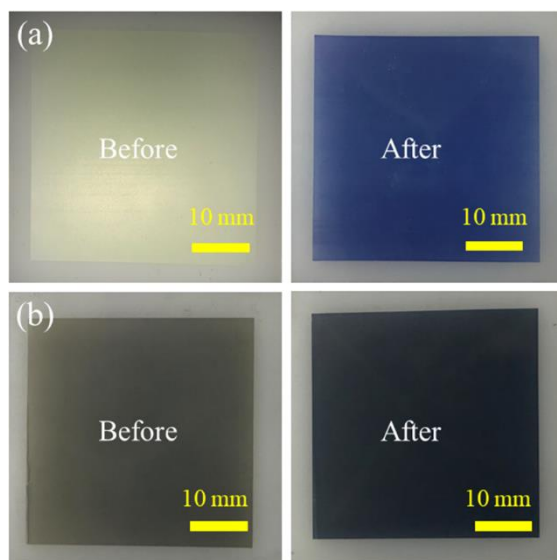


Fig. 15. Thin films of (a) WO_3 and (b) graphene/ WO_3 film with 15 wt.% graphite by NPDS; before and after photocatalytic experiment.

4.2 Mass of thin films

Before deposition of WO_3 and composite with graphite on PP, the mass of pure PP plate was measured. The thin films were fabricated by kinetic spraying of WO_3 and graphite particles. The mass of PP plate with thin films was again measured after

deposition. So, the mass of thin films can be easily obtained by the mass difference between after and before deposition which is shown in **Fig. 16**. As expected, the mass per cm^2 area of the composite thin films decreased with increasing graphite content because the density of graphite is lower than the density of WO_3 .

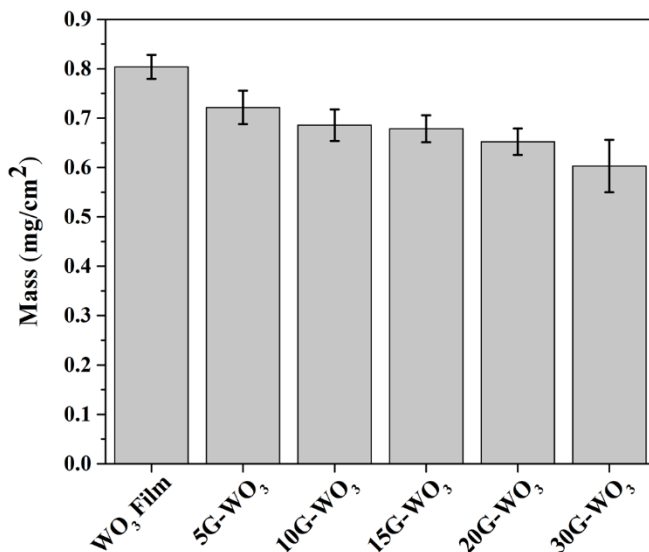


Fig. 16. Mass per unit area of thin films.

4.3 Confocal Microscopy

3D laser scanning confocal microscopy was used to measure the height difference between the non-coated and coated surfaces after film preparation. The laser beam was focused at some points on each sample, and the average value was calculated to measure the thickness of thin film. The average height is shown in **Fig. 17** for the WO_3 film and 15% graphite- WO_3 . **Fig. 18** shows the thickness of the thin films. The thicknesses of the fabricated films ranged from about 2 to 3 μm .

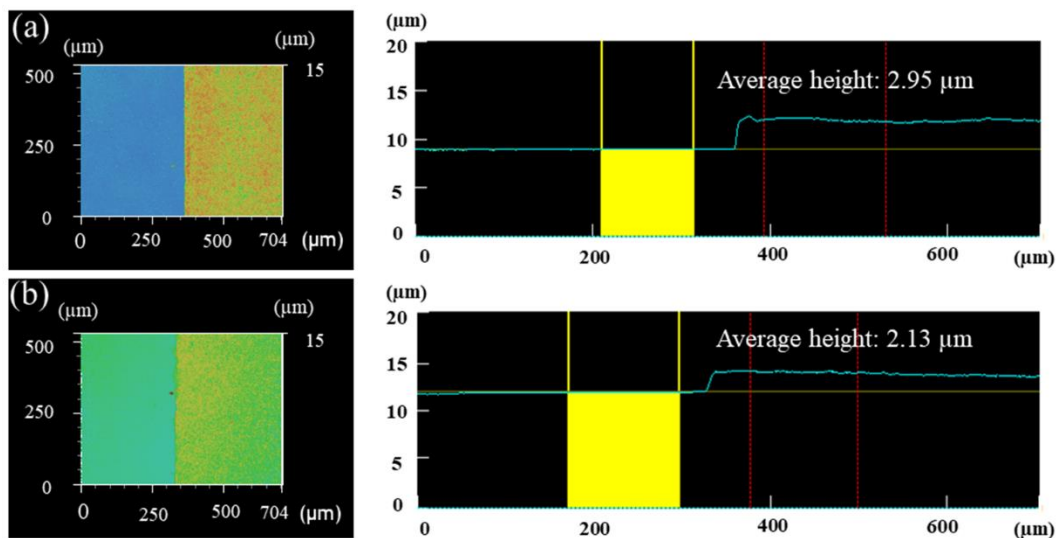


Fig. 17. Confocal microscopy images for (a) WO_3 film and (b) graphene/ WO_3 film with 15 wt.% graphite.

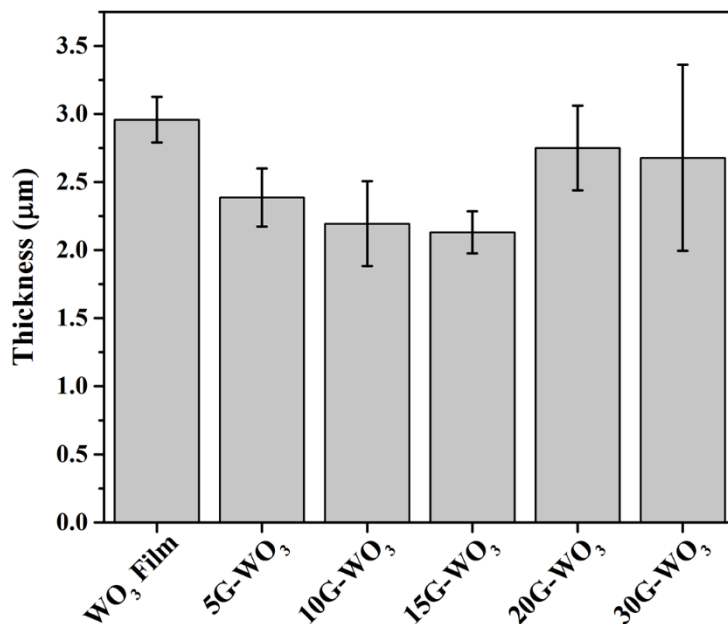


Fig. 18. Thickness of the as-deposited thin films.

4.4 FE-SEM

The surface morphologies of graphite particles, WO_3 powders, and deposited thin films were characterized by a field emission scanning electron microscope. **Fig. 19** shows the FE-SEM images for graphite and WO_3 particles. From **Fig. 19 (a-b)**, micro-sized particles of graphite and WO_3 powders can be clearly observed. The shape of the original particles is also clear from the images. **Fig. 20** depicts the SEM images of thin films by dry deposition process. **Fig. 20 (a)** with lower magnification clearly displays the WO_3 coating on PP plate. It can be noticeable from higher magnification of WO_3 film in **Fig. 20 (b)** that the large size WO_3 particles were fragmented into smaller sized particles by high kinetic energy during NPDS. The size of the WO_3 particles is roughly ~ 200 nm. Some of the WO_3 particles are more lower than this size. From **Fig. 20 (c)**, it can say that the deposition of 15 wt.% graphite/ WO_3 seems quite similar with only WO_3 film. However, when the magnification value is increased more, the small flake-like fragmented graphene structures less than $1\text{ }\mu\text{m}$ can evidently be found along with fragmented WO_3 particles from **Fig. 20 (d)**. The fragmentation happened because of high impact of graphite and WO_3 particles on PP via NPDS. The fragmented WO_3 particles are randomly distributed on the graphene sheets.

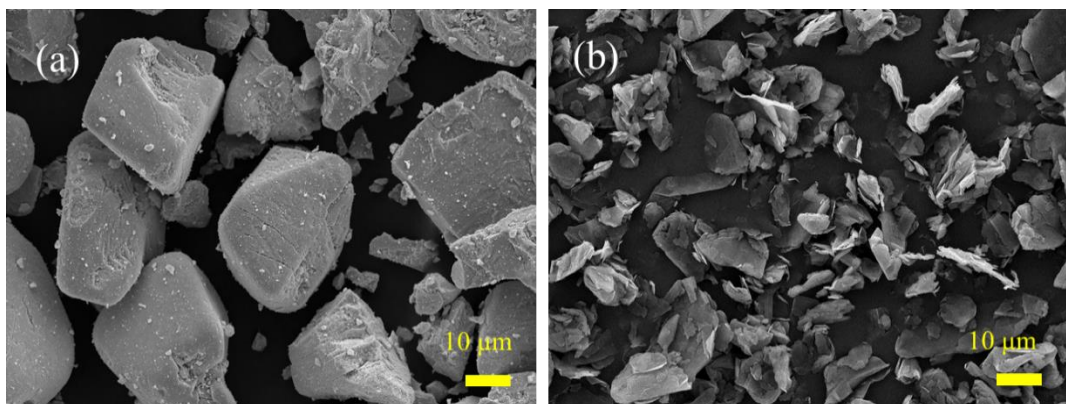


Fig. 19. FE-SEM images of (a) WO_3 powders, and (b) graphite powders.

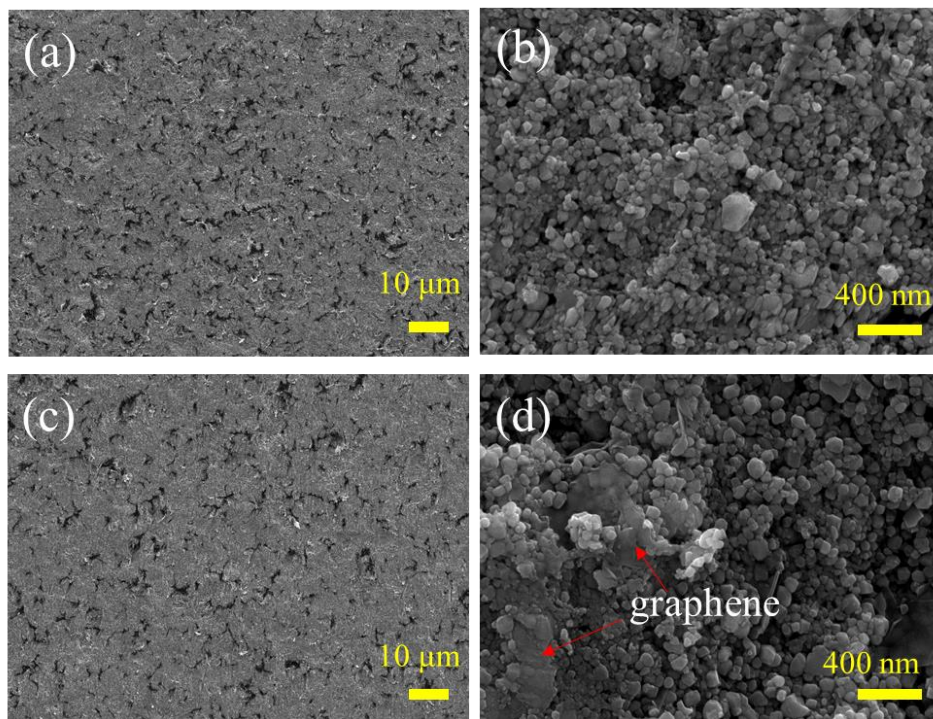


Fig. 20. FE-SEM images of thin films (a) & (b) WO_3 film, and (c) & (d) graphene/ WO_3 film with 15 wt.% graphite.

4.5 XRD

The crystalline structure and phase of the samples were examined by X-ray diffraction (XRD) analysis. XRD patterns of graphite powders, WO_3 powders, PP substrate, and deposited thin films prepared by NPDS were shown in **Fig. 21**. The XRD patterns were taken at the range of 10 to 50 two theta degree. The characteristic two strongest peaks of graphite powders correspond to the (002) and (004) planes of 2θ position at 26.4° and 54.52° , respectively. The WO_3 powders exhibited XRD peaks at 23.08° , 23.6° , 24.34° , 26.6° , 28.74° , 33.24° , 34.12° , 35.5° , 41.68° , 47.24° , 48.26° , 49.92° , and 55.58° that can be indexed to (002), (020), (200), (120), (112), (022), (202), (122), (222), (004), (040), (140), and (420) planes, respectively, indicating the good crystallinity of monoclinic WO_3 powders [10,47].

The XRD patterns were also analyzed for pure PP plate. PP shows some strong peaks. **Fig. 21 (d & e)** presents the diffraction patterns for WO_3 film and 15% graphite- WO_3 film. The PP peaks can also be observed from the peaks for thin film. By analyzing the peaks for WO_3 thin films, The monoclinic WO_3 crystal structure has not been changed into any other structures during NPDS. Most importantly, there was no graphite peak in the 15% graphite- WO_3 thin film compared with graphite powders, which was an indication that the pure graphite powders had been changed to graphene during NPDS.

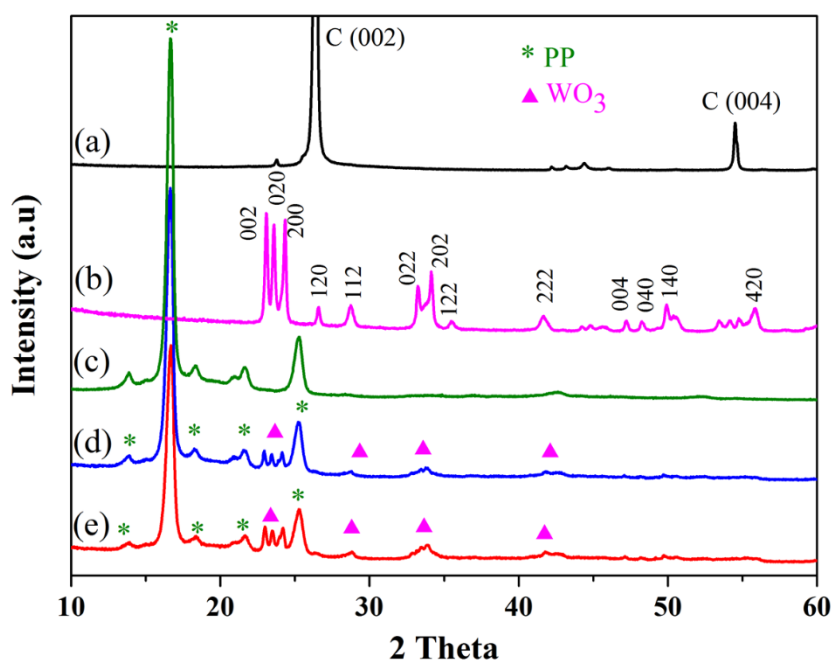


Fig. 21. XRD patterns of (a) graphite powders, (b) WO_3 powders, (c) PP, (d) WO_3 film, and (e) graphene/ WO_3 film with 15 wt.% graphite.

4.6 Raman Spectroscopy

Raman spectroscopy is a useful technique to analyze the formation of graphene and graphene/ WO_3 composites. Confocal Raman spectroscopic analysis was carried out to confirm the graphite and graphene structures of the deposited thin films. Basically, the existence of graphene in the composite can be confirmed by Raman analysis. Raman spectra of powders and as prepared thin films are displayed in **Fig. 22**. The Raman spectra for WO_3 powders shows three distinct peaks at ~ 271 , ~ 717 , and $\sim 810 \text{ cm}^{-1}$ and a weak signal at $\sim 328 \text{ cm}^{-1}$ in the region of $100\text{--}850 \text{ cm}^{-1}$ that corresponds to stretching and bending vibrations of O–W–O. The peaks centered at 717 and 810 cm^{-1} are due to the vibrational modes of the O–W–O bonds and the peaks located at 271 and 328 cm^{-1} are attributed to the bending modes of the O–W–O bonds in the monoclinic structure of WO_3 [48][71]. For graphite powders, the typical sp^2 bonded carbon atoms of hexagonal graphitic structure (D) and sp^2 carbon-type structure (G) bands are at 1350 cm^{-1} and 1580 cm^{-1} respectively. Also, the Raman peak for 2D band is at 2715 cm^{-1} [72–74]. All the Raman bands of WO_3 for WO_3 powders were observed in the WO_3 film and 15% graphite- WO_3 film. Small shifts for WO_3 in the composite film from 717 cm^{-1} to 712 cm^{-1} and from 810 cm^{-1} to 806 cm^{-1} may be due to interaction of WO_3 with graphene [20,21,55]. The characteristics peaks can be also found in the Raman spectrum of 15% graphite/ WO_3 film; besides, the distinctive D and G band of graphene are noticed, indicating the existence of graphene in the graphene/ WO_3 composite thin film. The peaks positions are also shown in **Fig. 21**. For the most important G and 2D peaks for the graphene structure, there was an upward shift in G peak position by $\sim 7 \text{ cm}^{-1}$ and a downward shift in 2D peak position by $\sim 31 \text{ cm}^{-1}$. These shifts are the difference between graphite and few layer graphene and confirmed the superior interactions

between WO_3 and graphene [19,49]. In addition, the downward shifting of the 2D peak suggested that the graphene flakes of the deposited thin film became thinner than the original graphite powders. Furthermore, this higher G peak shifting and lowered 2D peak shifting indicated that thinning occurred during deposition. Interestingly, the intensity ratio of the D and G peaks of 15% graphite/ WO_3 composite was higher than that of the graphite powders. This higher I_d/I_g also suggested fragmentation during deposition and deposition of defected flakes on PP [69]. The defects of the few-layer graphene flakes detected with higher I_d/I_g ratio allows superior interaction of WO_3 particles with graphene [75]. The interaction between graphene and WO_3 is very important for effective charge separation and transfer upon light excitation. In summary, the fragmentation of WO_3 and graphite particles occurred due to the high impact velocity of particles during deposition via NPDS. Also, the interaction between WO_3 and graphene after deposition on PP was confirmed for the composite thin film.

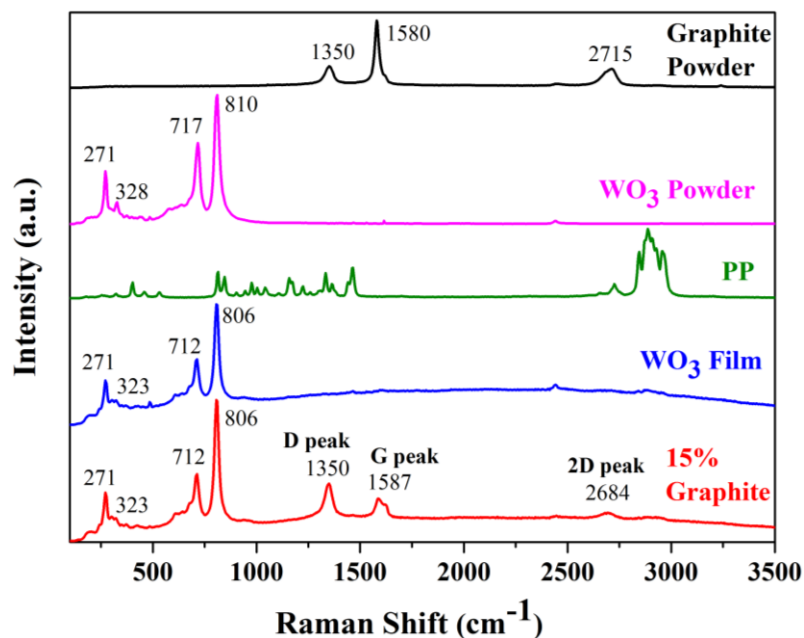


Fig. 22. Raman spectra of graphite powders, WO_3 powders, PP, WO_3 film, and graphene/ WO_3 film with 15 wt.% graphite.

CHAPTER 5

DISCUSSION

CHAPTER 5: DISCUSSION

In this research, a vacuum kinetic spray method was deployed successfully to deposit micron-sized graphite and WO_3 particles onto a polypropylene substrate at room temperature without using toxic chemicals. A few-layer graphene flake structured thin film was deposited directly by NPDS from micron-sized graphite powder in short process time. Micro-sized particles of WO_3 and graphite were fragmented to submicron or nano size particles by NPDS. This process required relatively low cost micro-sized powders as raw materials, and it is very simple to produce a composite thin film with mechanically mixed powder. Additionally, this process is environmentally friendly because it does not use toxic chemicals, and deposition was carried out at room temperature, so composite thin films were fabricated on a polymer substrate with low thermal resistance. With those advantages, NPDS can be an important process for preparation of a photocatalytic thin film.

As already discussed for photocatalytic activity analysis, the photocatalytic performance increased for WO_3 when graphite content increased from 0 to 15 wt.%. This enhanced performance may be mainly due to the superior interaction between graphene and WO_3 , the increased specific surface area, the efficient charge separation and the improved visible light absorption because of the incorporation of graphene. Firstly, the specific surface area of WO_3 could be increased due to the introduction of graphene. An increased surface area can increase surface active sites and can transport electrons easily and hence, photocatalytic activity can be improved [19,20,28,49,55]. Secondly, the electron-hole recombination could be delayed as the electrons could effectively be grafted and transferred by the graphene sheet. Thus, enhanced photocatalytic performance can be obtained. When WO_3 particles absorbed light greater than its band gap energy, electrons were excited to the conduction band, leaving holes in the valence band. In case of pure WO_3 , these photogenerated electrons could easily undergo

CHAPTER 5: DISCUSSION

with recombination process which decrease the dye degradation rate. However, for the composite of WO_3 with graphene, graphene can easily trap the electrons excited from the valence band of WO_3 . Most importantly, the positive aspect of graphene here is that it is a good electron acceptor. Graphene has also good electron transport capacity and as a result it can facilitate electron charge transfer and suppress recombination of electron-holes [50,76–78]. The trapped electrons on graphene reacting with oxygen can form O^{2-} . On the other hand, holes on the surface of WO_3 can convert oxygen to O^{2-} species as well which can react with water to convert it to OH^- and eventually, degrade the MB dye to convert it into harmless products. Finally, graphene can extend the light absorption region that can catch more photons in the visible range [22,45,79] and hence, improve the photo activity. However, further increase in graphite content beyond the optimal level resulted in decreased photocatalytic performance. The improvement was still greater than observed with the WO_3 thin film. Gan et al. reported that the degradation speed decreases after 7 wt.% graphene [47]. H. Sancan, H. Linfeng, L. Ziqi et al. [51] also explained that 2D $\alpha\text{-Fe}_2\text{O}_3$ hexagonal nanoplates/graphene composites with 5.0% graphene showed highest rate constant during RhB degradation. The rate constant for 8.0% graphene/ Fe_2O_3 was lower than that of 5.0% graphene/ Fe_2O_3 . Other researchers also describe similar results [24,27,80]. Here, the question is why the photocatalytic performance decreases with increasing graphene content after the optimal level. This might occur because increased graphene content can significantly reduce the light intensity because of shielding effect [21,26,81] and, hence, decrease the photocatalytic performance.

CHAPTER 6

CONCLUSION

CHAPTER 6: CONCLUSION

In summary, vacuum kinetic spray method presents a low cost, environmentally friendly, and simple thin film fabrication method to deposit graphene/ WO_3 thin film on a PP plate without toxic chemicals. Thin films can be easily prepared within very short time. This NPDS method is utilized effectively in the photocatalysis field using composite materials. The fabricated thin films were used in the photocatalytic activity for methylene blue dye degradation under visible light source for 2h. The prepared composite thin films showed excellent photocatalytic efficiency in comparison with pure WO_3 thin films. Among all the thin films, WO_3 film with 15 wt.% of graphite exhibited the highest photocatalytic performance for MB dye degradation in 2 hours. Hence, an optimal amount of graphene in graphene/ WO_3 composite thin films increases the performance of the photocatalyst. From the kinetic study, the chemical reaction rate for WO_3 film with 15 wt.% of graphite was about 1.5 times higher than that for pure WO_3 film. In addition, graphene/ WO_3 with 15% graphite shows very good repeatability, suggesting the prepared thin films with dry particle deposition method is very useful in using practical application. For the characterization, films were used for FE-SEM, XRD and Raman analysis. From FE-SEM, fragmentations of WO_3 and graphite particles were observed, and few layer graphene flake structure formation and the superior interaction between WO_3 and graphene structures were confirmed. Absence of graphite peaks was confirmed from XRD analysis. Most importantly, the existence of graphene with WO_3 was

CHAPTER 6: CONCLUSION

confirmed by Raman analysis. As the composite films showed good photostability and durability during recycling, they can be successfully fabricated within a very short time using the vacuum kinetic spray method and can effectively be used for photocatalytic dye degradation. It is suggested that NPDS would be a suitable process for constructing hybridized semiconductors for photocatalytic application

ACKNOWLEDGEMENT

This work was supported by the Energy Efficiency & Resources Core Technology Program of the Korea Institute of Energy Technology Evaluation and Planning (KETEP), granted financial source from the Ministry of Trade, Industry & Energy, Korea (No. 20142020103730) and was financially supported by National Research Foundation of Korea (NRF) grant (NRF-2018R1A2B6004012)

BIBLIOGRAPHY

- [1] F. Han, V.S.R. Kambala, M. Srinivasan, D. Rajarathnam, R. Naidu, Tailored titanium dioxide photocatalysts for the degradation of organic dyes in wastewater treatment: A review, *Appl. Catal. A Gen.* 359 (2009) 25–40.
- [2] S. Ahmed, M.G. Rasul, W.N. Martens, R. Brown, M.A. Hashib, Heterogeneous photocatalytic degradation of phenols in wastewater: A review on current status and developments, *Desalination*. 261 (2010) 3–18.
- [3] U.G. Akpan, B.H. Hameed, Parameters affecting the photocatalytic degradation of dyes using TiO₂-based photocatalysts: A review, *J. Hazard. Mater.* 170 (2009) 520–529.
- [4] S.-Y. Lee, S.-J. Park, TiO₂ photocatalyst for water treatment applications, *J. Ind. Eng. Chem.* 19 (2013) 1761–1769.
- [5] M.N. Chong, B. Jin, C.W.K. Chow, C. Saint, Recent developments in photocatalytic water treatment technology: A review, *Water Res.* 44 (2010) 2997–3027.
- [6] I.K. Konstantinou, T.A. Albanis, TiO₂-assisted photocatalytic degradation of azo dyes in aqueous solution: kinetic and mechanistic investigations: A review, *Appl. Catal. B Environ.* 49 (2004) 1–14.
- [7] R. Asahi, T. Morikawa, H. Irie, T. Ohwaki, Nitrogen-Doped Titanium Dioxide as Visible-Light-Sensitive Photocatalyst: Designs, Developments, and Prospects, *Chem. Rev.* 114 (2014) 9824–9852.
- [8] D. Chatterjee, S. Dasgupta, Visible light induced photocatalytic degradation of organic pollutants, *J. Photochem. Photobiol. C Photochem. Rev.* 6 (2005) 186–205.
- [9] Z. Li, S. Cong, Y. Xu, Brookite vs Anatase TiO₂ in the Photocatalytic Activity for Organic Degradation in Water, *ACS Catal.* 4 (2014) 3273–3280.

BIBLIOGRAPHY

- [10] J. Guo, Y. Li, S. Zhu, Z. Chen, Q. Liu, D. Zhang, W.-J. Moon, D.-M. Song, Synthesis of WO₃@Graphene composite for enhanced photocatalytic oxygen evolution from water, *RSC Adv.* 2 (2012) 1356–1363.
- [11] R. Li, Photocatalytic nitrogen fixation: An attractive approach for artificial photocatalysis, *Chinese J. Catal.* 39 (2018) 1180–1188.
- [12] R. de_Richter, T. Ming, P. Davies, W. Liu, S. Caillol, Removal of non-CO₂ greenhouse gases by large-scale atmospheric solar photocatalysis, *Prog. Energy Combust. Sci.* 60 (2017) 68–96.
- [13] S. Pavasupree, S. Ngamsinlapasathian, M. Nakajima, Y. Suzuki, S. Yoshikawa, Synthesis, characterization, photocatalytic activity and dye-sensitized solar cell performance of nanorods/nanoparticles TiO₂ with mesoporous structure, *J. Photochem. Photobiol. A Chem.* 184 (2006) 163–169.
- [14] A. Fujishima, K. Honda, Electrochemical photolysis of water at a semiconductor electrode, *Nature.* 238 (1972) 37—38. doi:10.1038/238037a0.
- [15] C. Dette, M.A. Pérez-Osorio, C.S. Kley, P. Punke, C.E. Patrick, P. Jacobson, F. Giustino, S.J. Jung, K. Kern, TiO₂ Anatase with a Bandgap in the Visible Region, *Nano Lett.* 14 (2014) 6533–6538.
- [16] I. Cesar, A. Kay, J.A. Gonzalez Martinez, M. Grätzel, Translucent Thin Film Fe₂O₃ Photoanodes for Efficient Water Splitting by Sunlight: Nanostructure-Directing Effect of Si-Doping, *J. Am. Chem. Soc.* 128 (2006) 4582–4583.
- [17] F. Meng, J. Li, S.K. Cushing, J. Bright, M. Zhi, J.D. Rowley, Z. Hong, A. Manivannan, A.D. Bristow, N. Wu, Photocatalytic Water Oxidation by Hematite/Reduced Graphene Oxide Composites, *ACS Catal.* 3 (2013) 746–751.
- [18] A. Devadoss, P. Sudhagar, S. Das, S.Y. Lee, C. Terashima, K. Nakata, A.

BIBLIOGRAPHY

- Fujishima, W. Choi, Y.S. Kang, U. Paik, Synergistic Metal–Metal Oxide Nanoparticles Supported Electrocatalytic Graphene for Improved Photoelectrochemical Glucose Oxidation, *ACS Appl. Mater. Interfaces*. 6 (2014) 4864–4871.
- [19] H. Huang, Z. Yue, G. Li, X. Wang, J. Huang, Y. Du, P. Yang, Ultraviolet-assisted preparation of mesoporous WO₃/reduced graphene oxide composites: superior interfacial contacts and enhanced photocatalysis, *J. Mater. Chem. A*. 1 (2013) 15110–15116.
- [20] L. Fu, T. Xia, Y. Zheng, J. Yang, A. Wang, Z. Wang, Preparation of WO₃-reduced graphene oxide nanocomposites with enhanced photocatalytic property, *Ceram. Int.* 41 (2015) 5903–5908.
- [21] B. Weng, J. Wu, N. Zhang, Y.-J. Xu, Observing the Role of Graphene in Boosting the Two-Electron Reduction of Oxygen in Graphene–WO₃ Nanorod Photocatalysts, *Langmuir*. 30 (2014) 5574–5584.
- [22] X. An, J.C. Yu, Y. Wang, Y. Hu, X. Yu, G. Zhang, WO₃ nanorods/graphene nanocomposites for high-efficiency visible-light-driven photocatalysis and NO₂ gas sensing, *J. Mater. Chem.* 22 (2012) 8525–8531.
- [23] S. Bai, K. Zhang, J. Sun, R. Luo, D. Li, A. Chen, Surface decoration of WO₃ architectures with Fe₂O₃ nanoparticles for visible-light-driven photocatalysis, *CrystEngComm*. 16 (2014) 3289–3295.
- [24] X. Bai, L. Wang, R. Zong, Y. Lv, Y. Sun, Y. Zhu, Performance Enhancement of ZnO Photocatalyst via Synergic Effect of Surface Oxygen Defect and Graphene Hybridization, *Langmuir*. 29 (2013) 3097–3105.
- [25] G.-J. Lee, J.J. Wu, Recent developments in ZnS photocatalysts from synthesis to photocatalytic applications — A review, *Powder Technol.* 318 (2017) 8–22.
- [26] K. Chang, Z. Mei, T. Wang, Q. Kang, S. Ouyang, J. Ye, MoS₂/Graphene

BIBLIOGRAPHY

- Cocatalyst for Efficient Photocatalytic H₂ Evolution under Visible Light Irradiation, *ACS Nano*. 8 (2014) 7078–7087.
- [27] X. Bai, L. Wang, Y. Zhu, Visible Photocatalytic Activity Enhancement of ZnWO₄ by Graphene Hybridization, *ACS Catal.* 2 (2012) 2769–2778.
- [28] Q. Li, B. Guo, J. Yu, J. Ran, B. Zhang, H. Yan, J.R. Gong, Highly Efficient Visible-Light-Driven Photocatalytic Hydrogen Production of CdS-Cluster-Decorated Graphene Nanosheets, *J. Am. Chem. Soc.* 133 (2011) 10878–10884.
- [29] M. Umadevi, A. Jegatha Christy, Synthesis, characterization and photocatalytic activity of CuO nanoflowers, *Spectrochim. Acta Part A Mol. Biomol. Spectrosc.* 109 (2013) 133–137.
- [30] D.B. Hernández-Uresti, A. Vázquez, D. Sanchez-Martinez, S. Obregón, Performance of the polymeric g-C₃N₄ photocatalyst through the degradation of pharmaceutical pollutants under UV–vis irradiation, *J. Photochem. Photobiol. A Chem.* 324 (2016) 47–52.
- [31] A.M. Al-Hamdi, U. Rinner, M. Sillanpää, Tin dioxide as a photocatalyst for water treatment: A review, *Process Saf. Environ. Prot.* 107 (2017) 190–205.
- [32] C. Zhou, G. Chen, Y. Li, H. Zhang, J. Pei, Photocatalytic activities of Sr₂Ta₂O₇ nanosheets synthesized by a hydrothermal method, *Int. J. Hydrogen Energy*. 34 (2009) 2113–2120.
- [33] M. Mishra, C. DM, alpha-Fe₂O₃ as a photocatalytic material: A review, *Appl. Catal. A Gen.* 498 (2015) 126–141.
- [34] P. Dong, B. Yang, C. Liu, F. Xu, X. Xi, G. Hou, R. Shao, Highly enhanced photocatalytic activity of WO₃ thin films loaded with Pt-Ag bimetallic alloy nanoparticles, *RSC Adv.* 7 (2017) 947–956.
- [35] M.C. Hidalgo, M. Maicu, J.A. Navío, G. Colón, Effect of Sulfate Pretreatment on Gold-Modified TiO₂ for Photocatalytic Applications, *J. Phys.*

BIBLIOGRAPHY

- Chem. C. 113 (2009) 12840–12847.
- [36] M. Mishra, H. Park, D.-M. Chun, Photocatalytic properties of Au/Fe₂O₃ nano-composites prepared by co-precipitation, *Adv. Powder Technol.* 27 (2016) 130–138.
- [37] D. Bi, Y. Xu, Synergism between Fe₂O₃ and WO₃ particles: Photocatalytic activity enhancement and reaction mechanism, *J. Mol. Catal. A Chem.* 367 (2013) 103–107.
- [38] N.A. Ramos-Delgado, M.A. Gracia-Pinilla, L. Maya-Treviño, L. Hinojosa-Reyes, J.L. Guzman-Mar, A. Hernández-Ramírez, Solar photocatalytic activity of TiO₂ modified with WO₃ on the degradation of an organophosphorus pesticide, *J. Hazard. Mater.* 263 (2013) 36–44.
- [39] K. Yao, P. Basnet, H. Sessions, G.K. Larsen, S.E.H. Murph, Y. Zhao, Fe₂O₃–TiO₂ core–shell nanorod arrays for visible light photocatalytic applications, *Catal. Today.* 270 (2016) 51–58.
- [40] M. Sabarinathan, S. Harish, J. Archana, M. Navaneethan, H. Ikeda, Y. Hayakawa, Highly efficient visible-light photocatalytic activity of MoS₂–TiO₂ mixtures hybrid photocatalyst and functional properties, *RSC Adv.* 7 (2017) 24754–24763.
- [41] I. Vamvasakis, I.T. Papadas, T. Tzanoudakis, C. Drivas, S.A. Choulis, S. Kennou, G.S. Armatas, Visible-Light Photocatalytic H₂ Production Activity of β -Ni(OH)₂-Modified CdS Mesoporous Nanoheterojunction Networks, *ACS Catal.* 8 (2018) 8726–8738.
- [42] Z. Li, B. Gao, G.Z. Chen, R. Mokaya, S. Sotiropoulos, G. Li Puma, Carbon nanotube/titanium dioxide (CNT/TiO₂) core–shell nanocomposites with tailored shell thickness, CNT content and photocatalytic/photoelectrocatalytic properties, *Appl. Catal. B Environ.* 110 (2011) 50–57.
- [43] T.-F. Yeh, J. Cihlář, C.-Y. Chang, C. Cheng, H. Teng, Roles of graphene

BIBLIOGRAPHY

- oxide in photocatalytic water splitting, *Mater. Today*. 16 (2013) 78–84.
- [44] W. Zhu, F. Sun, R. Goei, Y. Zhou, Facile fabrication of RGO-WO₃ composites for effective visible light photocatalytic degradation of sulfamethoxazole, *Appl. Catal. B Environ.* 207 (2017) 93–102.
- [45] H. Zhang, X. Lv, Y. Li, Y. Wang, J. Li, P25-Graphene Composite as a High Performance Photocatalyst, *ACS Nano*. 4 (2010) 380–386.
- [46] S. Pu, R. Zhu, H. Ma, D. Deng, X. Pei, F. Qi, W. Chu, Facile in-situ design strategy to disperse TiO₂ nanoparticles on graphene for the enhanced photocatalytic degradation of rhodamine 6G, *Appl. Catal. B Environ.* 218 (2017) 208–219.
- [47] L. Gan, L. Xu, S. Shang, X. Zhou, L. Meng, Visible light induced methylene blue dye degradation photo-catalyzed by WO₃/graphene nanocomposites and the mechanism, *Ceram. Int.* 42 (2016) 15235–15241.
- [48] X. Zhang, X. Lu, Y. Shen, J. Han, L. Yuan, L. Gong, Z. Xu, X. Bai, M. Wei, Y. Tong, Y. Gao, J. Chen, J. Zhou, Z.L. Wang, Three-dimensional WO₃ nanostructures on carbon paper: photoelectrochemical property and visible light driven photocatalysis, *Chem. Commun.* 47 (2011) 5804–5806.
- [49] A.A. Ismail, M. Faisal, A. Al-Haddad, Mesoporous WO₃-graphene photocatalyst for photocatalytic degradation of Methylene Blue dye under visible light illumination, *J. Environ. Sci.* 66 (2018) 328–337.
- [50] M.S.A. Sher Shah, A.R. Park, K. Zhang, J.H. Park, P.J. Yoo, Green Synthesis of Biphasic TiO₂–Reduced Graphene Oxide Nanocomposites with Highly Enhanced Photocatalytic Activity, *ACS Appl. Mater. Interfaces*. 4 (2012) 3893–3901.
- [51] H. Sancan, H. Linfeng, L. Ziqi, W. Swelm, A.A. A., C. Yongsheng, F. Xiaosheng, One-Step Hydrothermal Synthesis of 2D Hexagonal Nanoplates of α -Fe₂O₃/Graphene Composites with Enhanced Photocatalytic Activity,

BIBLIOGRAPHY

- Adv. Funct. Mater. 24 (2014) 5719–5727.
- [52] H. Choi, E. Stathatos, D.D. Dionysiou, Photocatalytic TiO₂ films and membranes for the development of efficient wastewater treatment and reuse systems, Desalination. 202 (2007) 199–206.
- [53] Z.A.M. Hir, P. Moradihamedani, A.H. Abdullah, M.A. Mohamed, Immobilization of TiO₂ into polyethersulfone matrix as hybrid film photocatalyst for effective degradation of methyl orange dye, Mater. Sci. Semicond. Process. 57 (2017) 157–165.
- [54] L. Lopez, W.A. Daoud, D. Dutta, B.C. Panther, T.W. Turney, Effect of substrate on surface morphology and photocatalysis of large-scale TiO₂ films, Appl. Surf. Sci. 265 (2013) 162–168.
- [55] R. Azimirad, S. Safa, Preparation of three dimensional graphene foam–WO₃ nanocomposite with enhanced visible light photocatalytic activity, Mater. Chem. Phys. 162 (2015) 686–691.
- [56] C. Su, B.-Y. Hong, C.-M. Tseng, Sol–gel preparation and photocatalysis of titanium dioxide, Catal. Today. 96 (2004) 119–126.
- [57] Z. Jiao, J. Wang, L. Ke, X.W. Sun, H.V. Demir, Morphology-Tailored Synthesis of Tungsten Trioxide (Hydrate) Thin Films and Their Photocatalytic Properties, ACS Appl. Mater. Interfaces. 3 (2011) 229–236.
- [58] A. Arfaoui, S. Touihri, A. Mhamdi, A. Labidi, T. Manoubi, Structural, morphological, gas sensing and photocatalytic characterization of MoO₃ and WO₃ thin films prepared by the thermal vacuum evaporation technique, Appl. Surf. Sci. 357 (2015) 1089–1096.
- [59] M.F. Abdel-Messih, M.A. Ahmed, A.S. El-Sayed, Photocatalytic decolorization of Rhodamine B dye using novel mesoporous SnO₂–TiO₂ nano mixed oxides prepared by sol–gel method, J. Photochem. Photobiol. A Chem. 260 (2013) 1–8.

BIBLIOGRAPHY

- [60] M.A. Fitri, M. Ota, Y. Hirota, Y. Uchida, K. Hara, D. Ino, N. Nishiyama, Fabrication of TiO₂-graphene photocatalyst by direct chemical vapor deposition and its anti-fouling property, *Mater. Chem. Phys.* 198 (2017) 42–48.
- [61] Y. Yuan, P. Shen, Q. Li, G. Chen, H. Zhang, L. Zhu, B. Zou, B. Liu, Excellent photocatalytic performance of few-layer MoS₂/graphene hybrids, *J. Alloys Compd.* 700 (2017) 12–17.
- [62] R.T. Sapkal, S.S. Shinde, T.R. Waghmode, S.P. Govindwar, K.Y. Rajpure, C.H. Bhosale, Photo-corrosion inhibition and photoactivity enhancement with tailored zinc oxide thin films, *J. Photochem. Photobiol. B Biol.* 110 (2012) 15–21.
- [63] Y.M. Hunge, M.A. Mahadik, A. V Moholkar, C.H. Bhosale, Photoelectrocatalytic degradation of oxalic acid using WO₃ and stratified WO₃/TiO₂ photocatalysts under sunlight illumination, *Ultrason. Sonochem.* 35 (2017) 233–242.
- [64] D.M. Chun, M.H. Kim, J.C. Lee, S.H. Ahn, TiO₂ coating on metal and polymer substrates by nano-particle deposition system (NPDS), *CIRP Ann.* 57 (2008) 551–554.
- [65] D.-M. Chun, S.-H. Ahn, Deposition mechanism of dry sprayed ceramic particles at room temperature using a nano-particle deposition system, *Acta Mater.* 59 (2011) 2693–2703.
- [66] S.H. Ahn, D.M. Chun, C.S. Kim, Nanoscale hybrid manufacturing process by nano particle deposition system (NPDS) and focused ion beam (FIB), *CIRP Ann.* 60 (2011) 583–586.
- [67] D.-M. Chun, J.-O. Choi, C. Lee, S.-H. Ahn, Effect of stand-off distance for cold gas spraying of fine ceramic particles (< 5 μm) under low vacuum and room temperature using nano-particle deposition system (NPDS), 2012.

BIBLIOGRAPHY

- [68] D.-M. Chun, J.-O. Choi, C.S. Lee, I. Kanno, H. Kotera, S.-H. Ahn, Nano-particle deposition system (NPDS): Low energy solvent-free dry spray process for direct patterning of metals and ceramics at room temperature, *Int. J. Precis. Eng. Manuf.* 13 (2012) 1107–1112.
- [69] M.N.E.A. Al Nasim, D.-M. Chun, Substrate-dependent deposition behavior of graphite particles dry-sprayed at room temperature using a nano-particle deposition system, *Surf. Coatings Technol.* 309 (2017) 172–178.
- [70] M.N.E.A. Al Nasim, D.-M. Chun, Formation of few-layer graphene flake structures from graphite particles during thin film coating using dry spray deposition method, *Thin Solid Films.* 622 (2017) 34–40.
- [71] O. Akhavan, M. Choobtashani, E. Ghaderi, Protein Degradation and RNA Efflux of Viruses Photocatalyzed by Graphene–Tungsten Oxide Composite Under Visible Light Irradiation, *J. Phys. Chem. C.* 116 (2012) 9653–9659.
- [72] A.C. Ferrari, Raman spectroscopy of graphene and graphite: Disorder, electron–phonon coupling, doping and nonadiabatic effects, *Solid State Commun.* 143 (2007) 47–57.
- [73] W. Hui, W. Yufang, C. Xuewei, F. Min, L. Guoxiang, Vibrational properties of graphene and graphene layers, *J. Raman Spectrosc.* 40 (2009) 1791–1796.
- [74] Y. Wang, D. Alsmeyer, R. McCreery, *Raman Spectroscopy of Carbon Materials: Structural Basis of Observed Spectra*, 1990.
- [75] G. Jeevitha, R. Abhinayaa, D. Mangalaraj, N. Ponpandian, Tungsten oxide-graphene oxide (WO₃-GO) nanocomposite as an efficient photocatalyst, antibacterial and anticancer agent, *J. Phys. Chem. Solids.* 116 (2018) 137–147.
- [76] N.R. Khalid, E. Ahmed, Z. Hong, L. Sana., M. Ahmed, Enhanced photocatalytic activity of graphene–TiO₂ composite under visible light irradiation, *Curr. Appl. Phys.* 13 (2013) 659–663.

BIBLIOGRAPHY

- [77] M.E. Khan, M.M. Khan, M.H. Cho, Fabrication of WO₃ nanorods on graphene nanosheets for improved visible light-induced photocapacitive and photocatalytic performance, *RSC Adv.* 6 (2016) 20824–20833.
- [78] Q. Xiang, J. Yu, M. Jaroniec, Synergetic Effect of MoS₂ and Graphene as Cocatalysts for Enhanced Photocatalytic H₂ Production Activity of TiO₂ Nanoparticles, *J. Am. Chem. Soc.* 134 (2012) 6575–6578.
- [79] Q.-P. Luo, X.-Y. Yu, B.-X. Lei, H.-Y. Chen, D.-B. Kuang, C.-Y. Su, Reduced Graphene Oxide-Hierarchical ZnO Hollow Sphere Composites with Enhanced Photocurrent and Photocatalytic Activity, *J. Phys. Chem. C.* 116 (2012) 8111–8117.
- [80] G.K. Pradhan, D.K. Padhi, K.M. Parida, Fabrication of α -Fe₂O₃ Nanorod/RGO Composite: A Novel Hybrid Photocatalyst for Phenol Degradation, *ACS Appl. Mater. Interfaces.* 5 (2013) 9101–9110.
- [81] H. Kim, G. Moon, D. Monllor-Satoca, Y. Park, W. Choi, Solar Photoconversion Using Graphene/TiO₂ Composites: Nanographene Shell on TiO₂ Core versus TiO₂ Nanoparticles on Graphene Sheet, *J. Phys. Chem. C.* 116 (2012) 1535–1543.